We are IntechOpen, the world's leading publisher of Open Access books Built by scientists, for scientists

6,900
Open access books available

185,000
International authors and editors

200M
Downloads

Our authors are among the

154
Countries delivered to

TOP 1%
most cited scientists

12.2%
Contributors from top 500 universities



WEB OF SCIENCE™

Selection of our books indexed in the Book Citation Index in Web of Science™ Core Collection (BKCI)

Interested in publishing with us?
Contact book.department@intechopen.com

Numbers displayed above are based on latest data collected.
For more information visit www.intechopen.com



8

Simulation of Three Dimensional Flows in Industrial Components using CFD Techniques

C. Bhasker
Hyderabad-500020
India

1. Introduction

1.1 Description of power/process plant

The schematic of coal fired power plant for electricity generation is shown in Fig-1, wherein fuel preparation is being made in grinding mills. The fuel from the mill outlet tubes will be transported to corner fired furnace as shown in Fig-2. The coal combustion in the furnace will takes place at 1500 deg C, wherein the tubes carrying water convert to saturated steam and enters in steam-drum. This steam in turn subjected turbine cylinders at different pressures through reheater/superheater, will generate electric power. Due to presence of high ash content in Indian coals, fluid transport devices often fail to perform with expected efficiencies. To troubleshoot these failures, industries are expected to integrate key technologies for design process through CAE-PLM concepts as suggested by Efim Korytnyi (1988). The traditional approach of taking a product from laboratory scales to pilot plants and then to develop the better efficient product is no longer attractive. While measurement probes provide point data, field information at multiple locations are often required to diagnose a problem fully. Success in this challenging environment hinges on leveraging the latest technology system based on CAE and multi-disciplinary coupled simulations as indicated by Pordal, et.al (2001) and Tylor B Thompson, et.al (1999).

2. CFD process

Today's design processes must be more accurate, while minimizing development costs to compete in a world economy. This forecast engineering companies to take advantage of design tools, which augment existing experience with empirical data. While minimizing cost, one tool which excels under these conditions are through CFD as discussed in technology road map towards chemical industries by Christopher Riff (2004). In general, CFD methods are used to understand the overall flow behavior of single/multi-component assemblies involves several steps like geometry modeling, computational mesh generation, and description of flow physics with turbulence, incorporating two-phase flow effects and visualization besides extending to multi-disciplinary areas like FSI and aero acoustics. CFD simulations are highly dependent on CAD model, which can be generated from programming/assembly drawings, are expected to be error free for evaluation of meaningful flow characteristics. Creation of component from simple to complex parts are generated using several commercial CAD software or programming is illustrated in Fig-3.

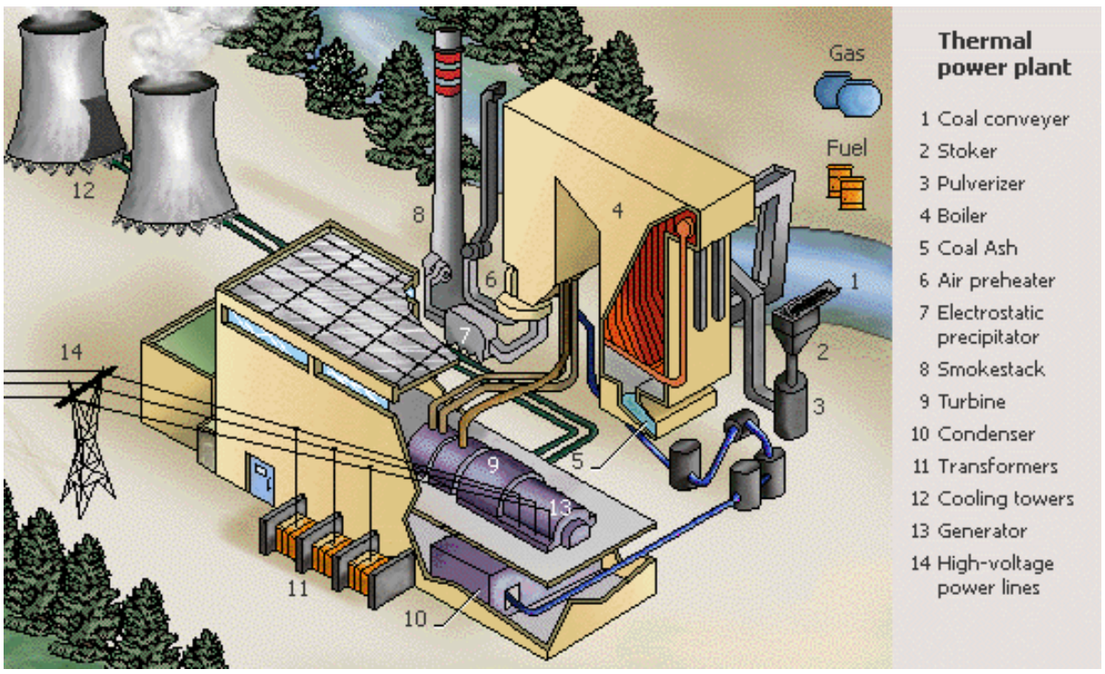


Fig. 1. Schematic of Coal fired Power Plant

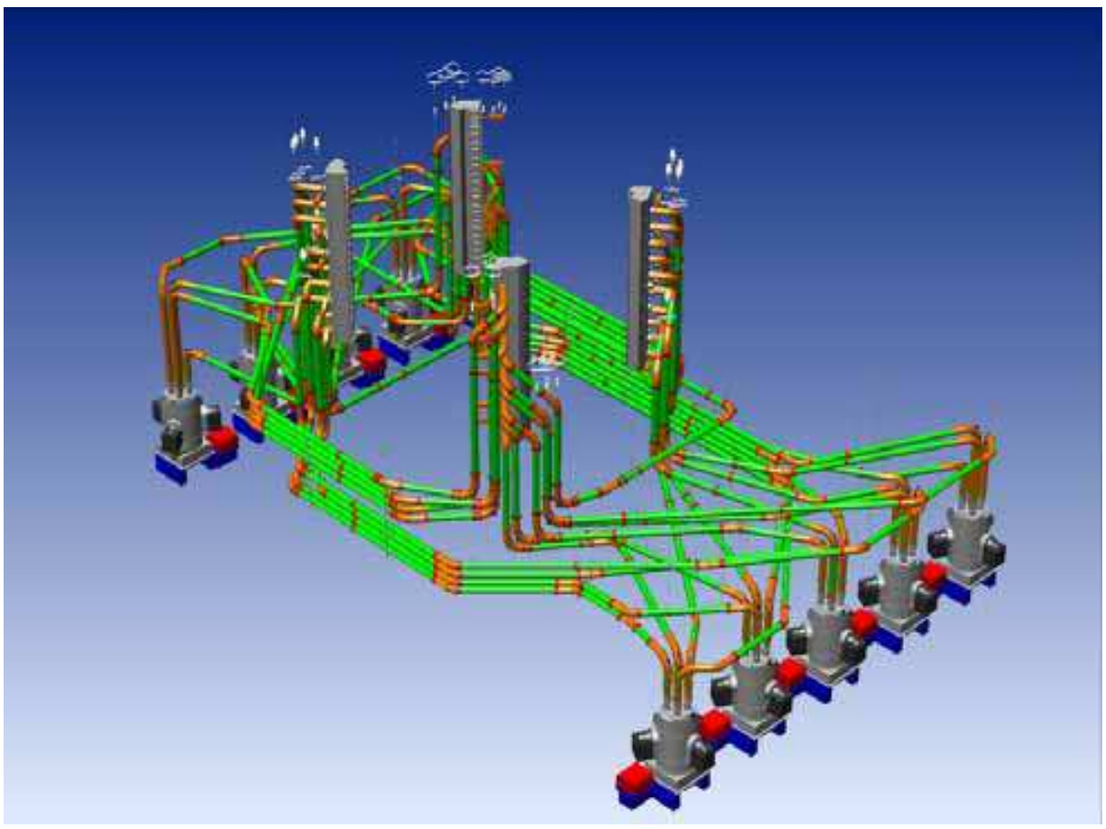


Fig. 2. Arrangement of fuel from mills to the furnace

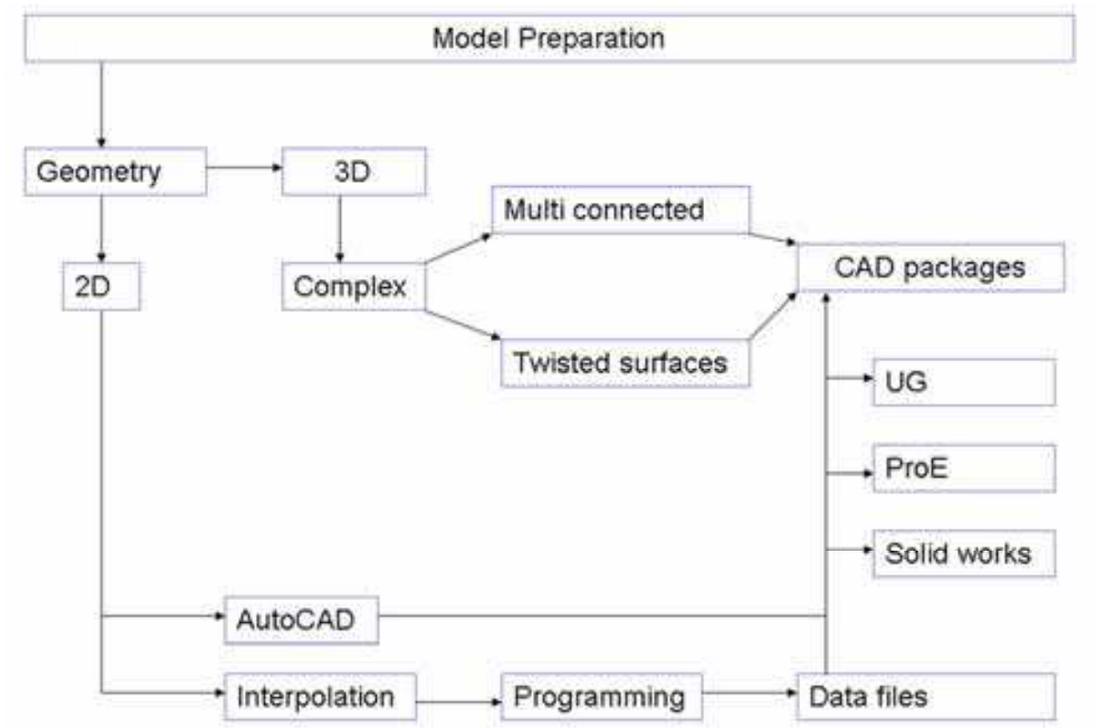


Fig. 3. Approach for creation of component geometries

The geometric shapes like cylinders, aerofoil and straight ducts can be generated through high level programming languages while linking its output to grid generation/flow simulation as discussed by C.Bhasker (2000). The disadvantage of this approach is of limited use and lacks graphic user interfaces for visualization of the component. If the geometries are complex assemblies involving complicated surface irregularities, solid modeling software provides effective tools for generation of three dimensional models accounting every detail of the component. The CAD software has powerful geometric engine provide variety of definition tools including fillet, shell, draft and feature based primitive icons to generate part modeling interactively were comprehensively discussed by Delli P (2007). CAD softwares includes powerful tools for capturing design intent in part features, which are easily edited and updated to support real-time modification processes. Using solid modeller softwares SDRC – I-DEAS and UG NX, several three dimensional component assemblies are created and exported to third party softwares for extraction of fluid portion for computational mesh generation.

3. Computational grid generation

At the core of CFD, computational grid is central element, which often considered as most important and time consuming part in simulation projects. The quality of the grid plays a direct role on the quantification of flow results, regardless of the flow solver used for simulation. The mesh generation concepts were comprehensively discussed by Thomson, JF (1985) and reviewed by Mazumdar. S (1994) has resulted to several commercial softwares which are being extensively used for several industrial components by Bhasker, C (2010a) was shown in Fig-4. The quality of mesh interms of size and density influences the accuracy,

convergence and speed of the numerical solution of fluid flow equations. As described in Fig-4 the computational mesh for component volume can be generated through unstructured, structured and hybrid method.

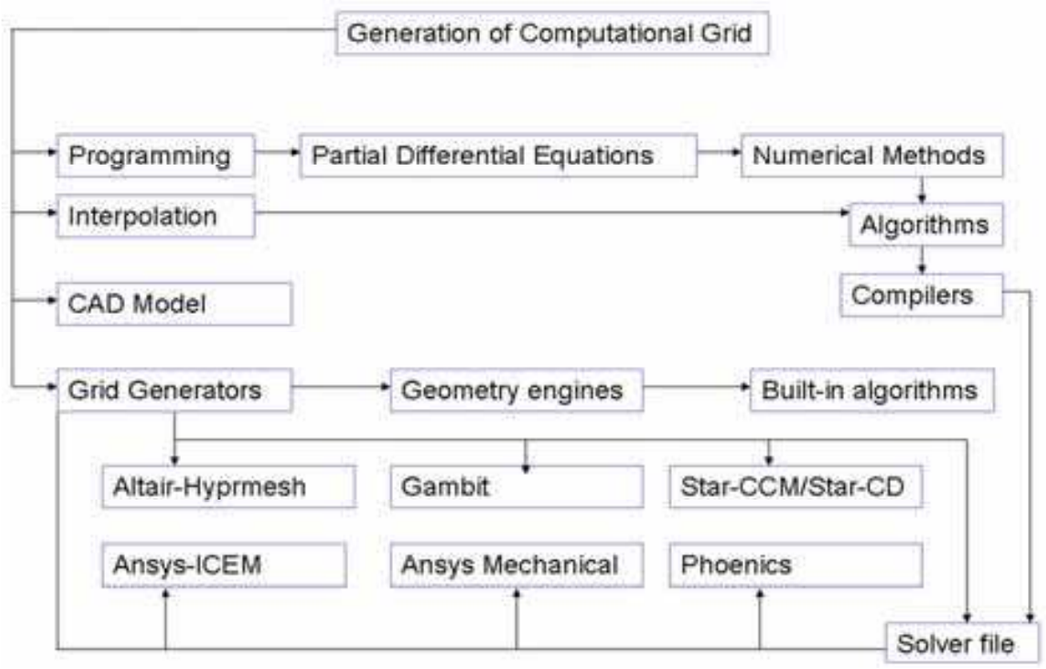


Fig. 4. Schematic of computational mesh generation

Unstructured grid methods utilize an arbitrary collection of elements to fill the domain automatically requires the volume bounded by error free surfaces. The unstructured mesh with tetra-hedral elements will have problems associated with large memories and lacks mesh refinement tools at desired locations in the computational domain is still preferred technique for the complex geometries. Using this type of mesh, parametric mesh generation for check valve has been developed by Iyer VK (2009) to estimate pressure drop under different opening conditions. In structured grid methods the grid is laid out in a regular repeating pattern called a block. These types of blocks utilize quadrilateral elements in 2D and hexahedral elements in 3D. Depending upon geometrical shape of the object, hexahedral elements with the combination of tetrahedral elements are generated in two different blocks of topologically connected boundaries. The accomplishment of computational meshes through high level programming requires numerical solutions to differential equation using interpolation or discretization using Finite volume/difference methods. To this effect, among several commercial grid generators, provides 2D/3D single and multiblock structured and unstructured meshing tools with the direct interface to popular flow solvers and applications are discussed in subsequent sections.

3.1 Structured grid generation using body fitted coordinates

The block grids using quadrilateral elements in 2D and hexahedral elements in 3D volume are generated through numerical solution to differential equations. If the geometries are not irregular, generation of body fitted coordinate grids are extensively discussed by Schuh

(1990) using the transformations from physical to computational domain as shown in the Fig-5.

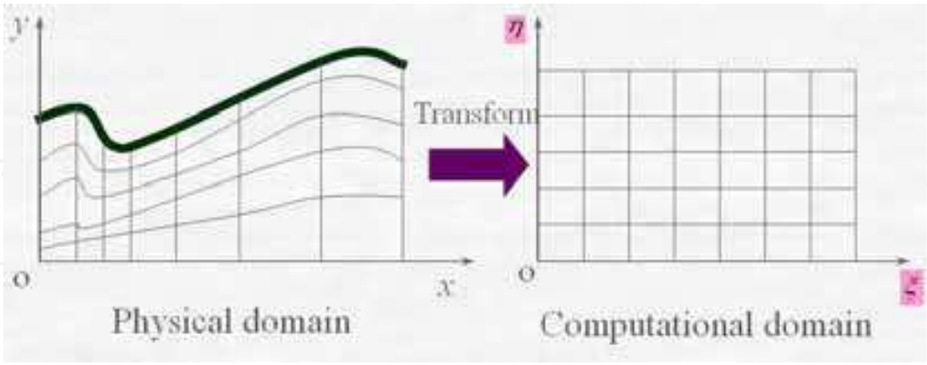


Fig. 5. Transformation of physical domain to computational domain

In the two-dimensions, the transformations in the mathematical form are represented as -

$$\frac{\partial f}{\partial x}=\frac{\partial f}{\partial \xi}\frac{\partial \xi}{\partial x}+\frac{\partial f}{\partial \eta}\frac{\partial \eta}{\partial x}=\xi_x\frac{\partial f}{\partial \xi}+\eta_x\frac{\partial f}{\partial \eta} \tag{1}$$

$$\frac{\partial f}{\partial y}=\frac{\partial f}{\partial \xi}\frac{\partial \xi}{\partial y}+\frac{\partial f}{\partial \eta}\frac{\partial \eta}{\partial y}=\xi_y\frac{\partial f}{\partial \xi}+\eta_y\frac{\partial f}{\partial \eta} \tag{2}$$

Substitution of these derivatives in the Poisson equation, the transformed equation will results to -

$$\alpha\frac{\partial^2\xi}{\partial x^2}+2\beta\frac{\partial x}{\partial \xi\partial \eta}+\gamma\frac{\partial^2\eta}{\partial x^2}=-J^2\left(P\frac{\partial x}{\partial \xi}+Q\frac{\partial x}{\partial \eta}\right) \tag{3}$$

$$\alpha\frac{\partial^2\xi}{\partial y^2}+2\beta\frac{\partial y}{\partial \xi\partial \eta}+\gamma\frac{\partial^2\eta}{\partial y^2}=-J^2\left(P\frac{\partial y}{\partial \xi}+Q\frac{\partial y}{\partial \eta}\right) \tag{4}$$

$$\alpha=\frac{\partial^2 x}{\partial \xi^2}+\gamma\frac{\partial^2 x}{\partial \eta^2}\quad;\quad \gamma=\frac{\partial^2 y}{\partial \xi^2}+\gamma\frac{\partial^2 y}{\partial \eta^2} \tag{5}$$

$$J=\frac{\partial(x,y)}{\partial(\xi,\eta)}=\frac{\partial x}{\partial \xi}\frac{\partial y}{\partial \eta}-\frac{\partial x}{\partial \eta}\frac{\partial y}{\partial \xi} \tag{6}$$

and the control functions P,Q in terms of transformed coordinates are written as

$$P(\xi,\eta)=\sum_{i=1}^{N}-a_i sign(\xi-\xi_i)e^{-c_i|\xi-\xi_i|}\quad-\quad\sum_{j=1}^{M}b_i sign(\xi-\xi_i)e^{-d\left|(\xi-\xi_i)^2+(\eta-\eta_i)^2\right|^{\frac{1}{2}}} \tag{7}$$

$$Q(\xi,\eta)=\sum_{i=1}^{N}-a_i sign(\eta-\eta_i)e^{-c_i|\eta-\eta_i|}\quad-\quad\sum_{j=1}^{M}b_i sign(\eta-\eta_i)e^{-d\left|(\eta-\eta_i)^2+(\xi-\xi_i)^2\right|^{\frac{1}{2}}} \tag{8}$$

Where a,b,c,d are positive integers which control the magnitude of attraction towards line and point. Negative value of a and b result in the repulsion from the lines and points. Boundaries of cylinder and aerofoil are seen in the Fig-6. To account curvature and spacing, the derivatives of control functions are written as –

$$P(\xi,\eta) = -\frac{\frac{\partial x}{\partial \xi} \bullet \frac{\partial^2 x}{\partial \xi^2}}{\left|\frac{\partial x}{\partial \xi}\right|^2} - \frac{\frac{\partial x}{\partial \xi} \bullet \frac{\partial^2 x}{\partial \eta^2}}{\left|\frac{\partial x}{\partial \eta}\right|^2} \quad ; \quad \left|\frac{\partial x}{\partial \xi}\right| = \left[\frac{\partial x}{\partial \xi} \bullet \frac{\partial x}{\partial \xi}\right]^{\frac{1}{2}} \tag{9}$$

$$Q(\xi,\eta) = -\frac{\frac{\partial y}{\partial \eta} \bullet \frac{\partial^2 y}{\partial \eta^2}}{\left|\frac{\partial r}{\partial \xi}\right|^2} - \frac{\frac{\partial y}{\partial \eta} \bullet \frac{\partial^2 y}{\partial \xi^2}}{\left|\frac{\partial y}{\partial \xi}\right|^2} \quad ; \quad \left|\frac{\partial y}{\partial \eta}\right| = \left[\frac{\partial y}{\partial \eta} \bullet \frac{\partial y}{\partial \eta}\right]^{\frac{1}{2}} \tag{10}$$

The effect of control functions P, Q with attraction of points (fine grid points) towards the boundaries. Such types of grids close to solid boundaries are essential in CFD simulation for accurate estimation of viscous losses. In order to generate body fitted computational mesh, elliptic partial differential equations with control functions are solved numerically using finite volume techniques. The control functions clusters the mesh points towards solid boundaries very closely to account viscous losses. An interactive program has been developed for generation of body fitted coordinated grid for cylinder and aerofoil whose output has been visualised in the graphic software Tecplot3D. The body fitted computational mesh data from the program for a rod-aerofoil with boundary layer thickness towards solid boundaries are shown in Fig-6 and the detailed derivations and program code structure is available in the presentation material by Bhasker (2010b).

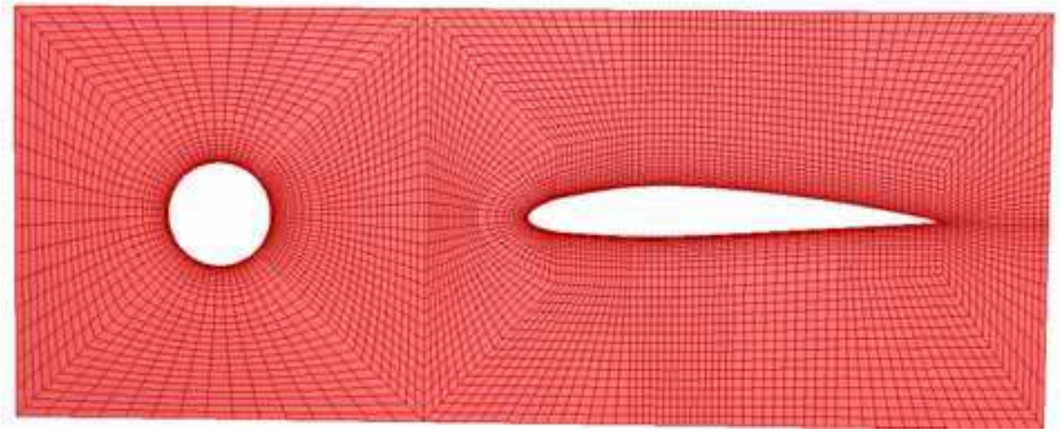


Fig. 6. Body fitted CFD mesh for rod-aerofoil using programming approach

When the geometries are irregular and multi-connected, the programming approach is limited usage and algorithms for multiblock structured grid generation schemes were developed by Spekreijse (1966) are implemented in commercial software, which provides more user friendly under Graphic User Interface – GUI environment with powerful geometric engine for CAD repair and multi-block grid generation, with choice of elements and different distribution laws for mesh density.

3.2 Structured multi-block grid generation

The geometry of fuel preparation device called beater wheel mill used for power generation has been considered from the experimental investigation by Founti (1995) for flow simulation using multiblock structured grid generation. The geometrical details and block decomposition around solid objects like impeller vanes baffle plates in the classifier, wherein flow is subjected to impeller blades for crushing the coals into fine particles. The flow from the impeller outlet enters mill chamber travels upwards through convergent duct and enters in the classifier region from baffle plates. In order to carry out flow simulation, mill geometry in 2D plane has been created and decomposed for mesh generation using commercial grid generator as shown in Fig 7(a).

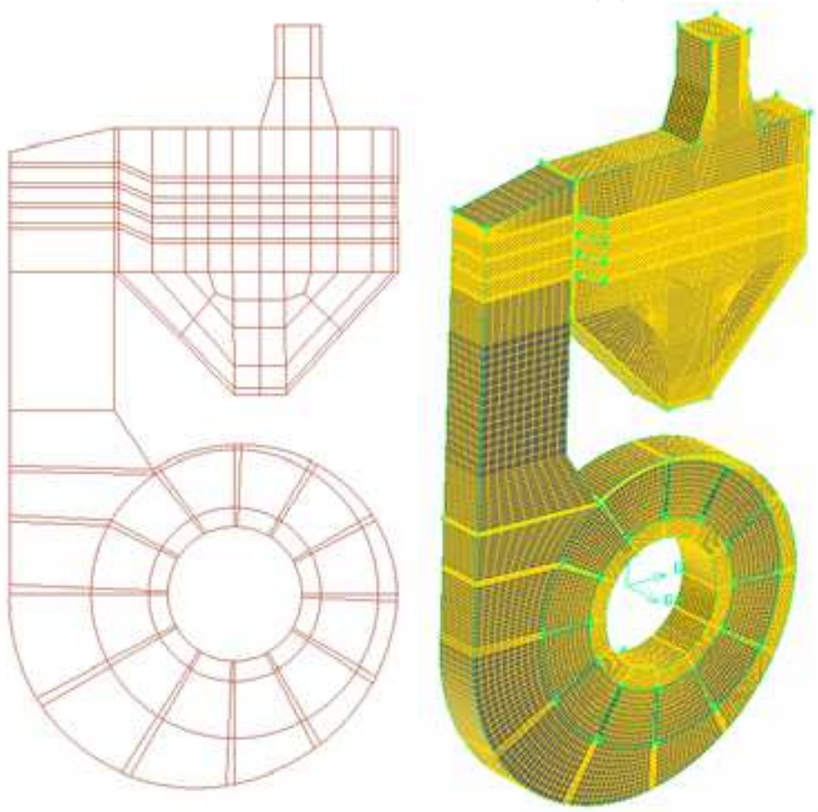


Fig. 7. (a-b) Multiblock structured grid for industrial component

In order to generate computational mesh for the mill geometry shown, the component has grouped into three parts impeller, converging duct and classifier which can be toggled through blank and unblank options. In the computational domain, 2d mesh generation has been started from the small cell using quad elements. To avoid mixed elements, mesh style algorithms are properly chosen to map rectangular mesh. In order to have uniform mesh at neighboring cell, mesh density is varied in the flow direction. In this process, the mesh densities at mating edge across two cells are equivalenced. In this process, 2d quad elements at all the cells present in the computational domain are filled and equivalenced the edges so that no duplicate nodes are present across mating edges of cells. After checking the mesh quality, computational mesh was dragged in z direction for specified distance to generate

three dimensional meshes as shown in the Fig 7(b). The flow simulation through CFD coarse grid was extensively discussed by Anagnotopoulos J (1997) for partial geometry of the mill, which in turn was extended for detailed investigation by Bhasker (2008) to simulate the air flow from mill inlet to classifier outlet location.

3.3 Emerging trends in grid generation

Structured grid forms through building blocks, which will have six neighbor cells possess excellent numerical properties, when the flow is aligned with the grid. Hexahedral elements, which are efficient at filling space, support a high amount of skewness and stretching before the solution is significantly effected. Alternatively, computational mesh can be generated for complex shaped object through automatically using tetrahedral element, which has four neighbor cells. But, the triangle and tetrahedral elements have the problem that they do not stretch or twist well, therefore, the grid is limited to be isotropic, i.e. all the elements have the same size and shape. Ideally, flow should be perpendicular to the element surfaces. Hence, tetrahedrons are the least ideal computational cell and they are inefficient at filling space. Though volume mesh with tetra-hedral elements generates faster, but the simulation of flow equations require more memory and have longer execution times than structured grid solvers. Hexahedra elements are an improvement, but they are difficult and expensive to generate for complex geometries.

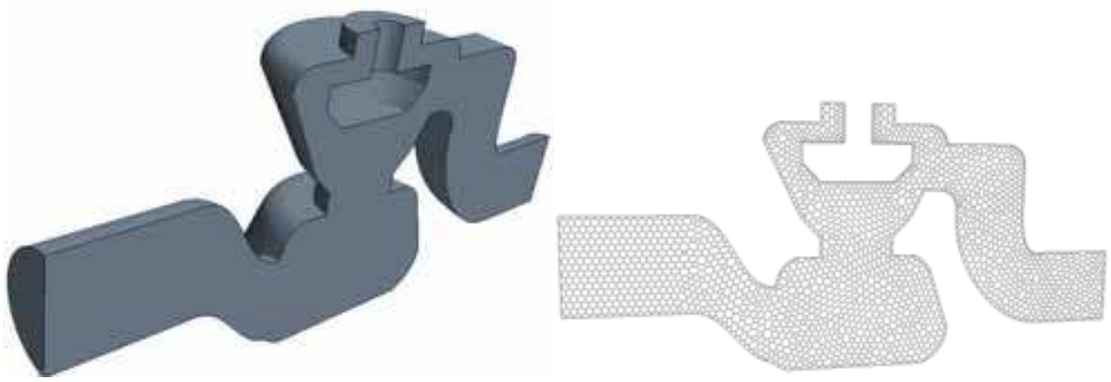


Fig. 8. Polyhedral Mesh for the valve (a) geometry (b) Mesh

To overcome these difficulties, CFD solvers have developed new type of element is called polyhedral as discussed by Stephen Fergusen (2005). Polyhedral cells possess excellent numerical properties including good accuracy using finite volume discretizations and well connections with neighboring cells. Polyhedral mesh cell counts are much smaller than tetrahedral meshes with equivalent accuracy. The flow solvers Star-CCM and Fluent use polyhedral meshes for flow simulation. In order to generate polyhedral meshes for CFD flow simulation, the geometry of control valve is shown in Fig.8 (a) was imported. On visualization, it is observed that surface representation of geometry through triangle definition was coarsely faceted.

In order to improve surface quality, the solid boundary surfaces are need to be broken so that mesh refinements/clustering can be created at desired locations. Using this option, geometry of component was split at an angle of 45^0 to obtain several boundary surfaces. These boundaries are carefully visualized and grouped into the regions like inlet, exit, valve body and symmetry surfaces. In order to improve/generate the surface/volume mesh

quality, the suitable inputs related to surface curvature, growth rate, proximity, base size, number of prism layers, prism layer stretching and relative thickness values are defined. For the provided flow conditions, flow simulation has been carried out on this polyhedral mesh shown in Fig-8(b) for several flow characteristics and estimation of pressure drop evaluation across control valve inlet/exit locations by Bhasker (2010c).

4. Fluid mechanics – effect of turbulence

The transport of fluid comprises gases/liquid from one component to other in power/process equipment are described through mass, moment and energy conservation principles. The Navier Stokes (transport) equations are derived from these principles are discussed by Hoffman, K.A [1993) are represented mathematically as-

$$\frac{\partial \rho\phi}{\partial t} + div\left(\rho\phi\vec{u}\right) = div\left(\Gamma grad\phi\right) + q_{\varphi} \tag{11}$$

The terms on Left Hand Side – LHS defines acceleration of flow over time with inertia depends on the sum of the external forces, diffusion and sources acting on the fluid element. If the value of φ is 1, the eqn. (11) results to continuity equation. The value of φ is either u or v or w, the above eqn. describes momentum equation in x, y, z directions. The value of φ is h then the above eqn. yields to energy equation. Two important material properties of fluid i.e., density and viscosity, whose ratio times characteristic flow velocity and length are defined as Reynolds number. This non-dimensional quantity is the ratio of inertial forces to viscous forces, whose magnitude depends upon flow disturbances can changes from laminar to turbulent. In other words, if the Reynolds Number is small, then the flow will be laminar and the flow progresses in layers. If the Reynolds Number is large flow then the flow will be turbulent and there will be a mixing of flow layers with large eddies are illustrated through cigarette smoke in Fig-9 by Sodja, J (2007).

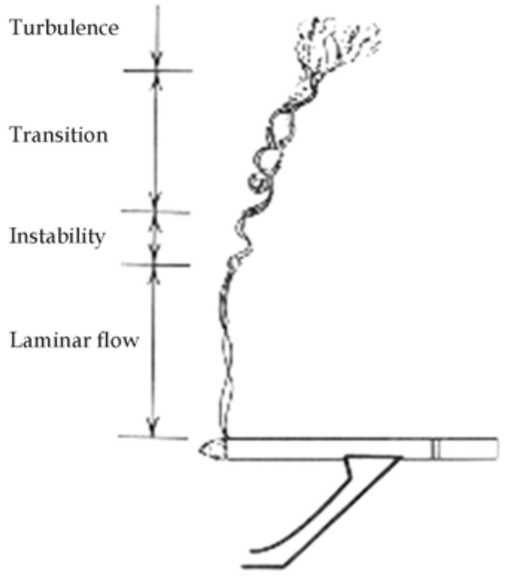


Fig. 9. Illustration of turbulent flow from cigarette smoke

The flow consists of a spectrum of different scales in turbulent flow, largest eddies are the order of geometry scales and breaks into smaller as time progress. At the other end of the spectra, the smallest eddies by viscous forces are dissipated into internal energy. Even though turbulence is chaotic, its characteristics are determined through Navier-Stokes equations. The turbulent is dissipative, which means that kinetic energy in the small eddies are transformed into internal energy. The small eddies receive the kinetic energy from slightly larger eddies. The slightly larger eddies receive their energy from even larger eddies and so on. In order to resolve wide spectrum of scales in turbulent eddies, normally two approaches are employed and are discussed in detail by Zhiqiang Z (2007). The first approach is Direct Numerical simulation – DNS, wherein the range of eddy size varies as small as the Kolmogorov scale in turbulent flow. This requires dense mesh points for proper resolution and its solution depends on heavy computational resources, expensive, time consuming process and very rarely used simulation technique. The other approach generally used for most of the applications are Reynolds' averaging process described by Shao (2009), wherein flow variables are decomposed into mean and fluctuating components as -

$$u_i = \bar{u}_i + u_i' \tag{12}$$

Where i=1.2,3 denotes in x, y, z direction. Like wise the pressure and other scalars can be expressed as

$$\phi = \bar{\varphi} + \phi' \tag{13}$$

Substituting flow variables in the form into the instantaneous continuity and momentum equations and taking a time (or ensemble) average (and dropping the overbar on the mean velocity) yields to

$$\frac{\partial \rho}{\partial t} + \frac{\partial}{\partial x_i}(\rho u_i) = 0 \tag{14}$$

$$\frac{\partial}{\partial t}(\rho u_i) + \frac{\partial}{\partial x_j}(\rho u_i u_j) = -\frac{\partial p}{\partial x_i} - \frac{\partial}{\partial x_j}\left[\mu\left(\frac{\partial u_i}{\partial x_j} + \frac{\partial u_j}{\partial x_i} - \frac{2}{3}\delta_{i,j}\frac{\partial u_l}{\partial x_l}\right)\right] + \frac{\partial}{\partial x_j}\left(\overline{-\rho u_i' u_j'}\right) \tag{15}$$

Eqn (14-15) are called (RANS) equations. The term $\overline{\rho u_i' u_j'}$ in the eqn (15) results from averaging process is called Reynolds' Stress. With the help of Boussinesq hypothesis to relate the Reynolds stresses, choosing Kronecker delta δ=1 if $i=j$ and $\overline{u_i' u_i'} = 2k$ the Reynold's stress term in the eqn (15) is rewritten as -

$$\overline{-\rho u_i' u_i'} = \mu_t\left(\frac{\partial u_i}{\partial x_j} + \frac{\partial u_j}{\partial x_i}\right) - \frac{2}{3}\left(\rho k + \mu_t \frac{\partial u_k}{\partial x_k}\right)\delta_{i,j} \tag{16}$$

Where μ_t is turbulent viscosity. To resolve turbulence viscosity and Reynolds' stresses, eddy viscosity models based on Boussinesq hypothesis will leads to zero, one and two equation turbulence models and Reynolds's Stress models – RSM. The strength and weakness of these models for prediction of turbulence effects are extensively reviewed by Davidson (2003). Whenever non-isotropic effects in turbulence are important use of higher

models like v^2-f is preferable to predict separation near the wall. When the fluid flow is subjected to rotating components, Large Eddy Simulation –LES or Detached Eddy Simulations - DES are employed to evaluate flow characteristics as a function of turbulence viscosity and energy dissipation. These models are based on filtered equations, still require finer meshes and solve RANS calculations in transient mode. In the simulation of turbulent flows, accurate estimation of pressure drop infact highly dependent on usage of turbulence model with smooth/rough wall functions. The variation of pressure influence surfaces roughness and can alter structural stresses. Description of these models are highly mathematical nature and its detailed derivations are available in the technical paper by Durbin P.A. (1995) and text book by Wilcox (1999). An application of turbulent flows in complex components of industrial equipments are discussed in the case study -1 & 2.

5. CFD Solvers – Finite Volume Algorithms (FVM)

As discussed in the previous section, whether working fluid is a compressible or incompressible and laminar or turbulent, its dynamics are described by mass, momentum and energy equations. However its complexities depends upon consideration of the external forces due to presence of discrete particles, fluid-solid interactions and aero acoustics besides incorporating thermal phenomena involving different modes of heat transfer mechanism in the simulation. FVM is used to discretize Navier Stokes equations (11) numerically to solve for several flow variables on high speed digital devices as discussed by Petersburg (2004). The integration of transport equation over the control volume, after applying Gauss divergence theorem can be written as

$$\int_{CV} \frac{\partial \rho\phi}{\partial t} dV + \oint_S (\rho\phi\vec{u}) \bullet \vec{n} dS = \int_S (\Gamma grad\phi) \bullet dS + \int_{CV} q_\phi dV \tag{17}$$

The control volume of typical cuboids with P as its center are surrounded by six faces defined as n – North, s – South, e-East, w-West, t-Top and b-Bottom. The face centers n, s, e, w, t and b are located at the intersection of the lines joining the midpoint of the opposite edges. All variables are stored either in collocated or staggered nodes in the finite volume cell to address pressure-velocity coupling. If the flow is steady, in the LHS of eqn (17) first term vanishes. On RHS of above eqn. if q is constant in the source term and linear, then the volume integral can be approximated about p as

$$\int_{CV} q_\phi dV = \overline{q} Vol(CV) \approx \quad q_p Vol(CV) \tag{18}$$

If q is bilinear, interpolation of q at more points of control volume can is approximated as

$$\int_{CV} q_\phi dV = \frac{\Delta x \Delta y}{36} \left[16q_p + 4q_s + 4q_n + 4q_e + 4q_w + q_{se} + q_{sw} + q_{ne} + q_{nw} \right] \tag{19}$$

Now to approximate surface integral on LHS of eqn (17), the net flux through CV boundary is the sum of integrals over the faces implies

$$\int_s (\rho\phi\vec{u}) \bullet \vec{n} dS = \int_s f \bullet \vec{n} dS = \sum_k \int_{s_k} f dS \qquad where \quad f = \rho\phi\vec{u} \tag{20}$$

Considering east face, assuming dependent variables like velocity/density (f) at cell points and if the points ne, e and se known, the function f with unknown variable φ can be approximated through Simpsons rule as

$$\int_S f dS \approx \frac{S_e}{6}\left(f_{ne} + 4fe + f_{se}\right) \tag{21}$$

To determine f with the unknown φ, interpolations like, unwind – (UDS), central differencing–(CDS) and quadratic upwind interpolation–(QUICK) techniques are shown in Fig-10 are used to develop the algorithms. In the case of upwind difference, the value of φ at location e will be

$$\phi_e = \begin{cases} \phi_p \; if \; \left(\vec{u} \bullet \vec{n}\right)_e \rangle 0 \\ \phi_e \; if \left(\vec{u} \bullet \vec{n}\right)_e \langle 0 \end{cases} \tag{22}$$

this scheme is of first order, the solution is numerically diffusive and generally not recommended. The approximation of φ at location e in the case of central difference scheme is.

$$\phi_e = \phi_E \lambda_e + \phi_p\left(1 - \lambda_p\right) \tag{23}$$

Which is a second order, still produce oscillations.

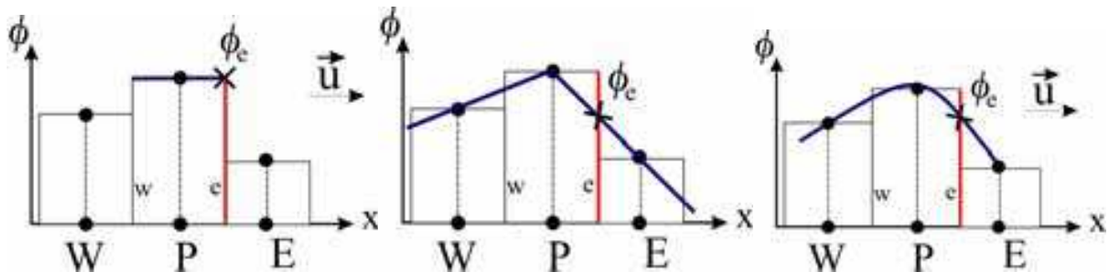


Fig. 10. Illustration of UDS, CDS and QUICK Interpolation Schemes

The approximation using QUICK

$$\phi_e = \begin{cases} \phi_p + g_1\left(\phi_e - \phi_p\right) + g_2\left(\phi_p - \phi_w\right) & if \quad u_x \rangle 0 \\ \phi_e + g_3\left(\phi_p - \phi_e\right) + g_4\left(\phi_e - \phi_p\right) & if \quad u_x \langle 0 \end{cases} \tag{24}$$

Where g is coefficients in terms of nodal coordinates and the scheme is third order and aimed to provide accurate estimates. In the QUICK scheme, one adds one point in each direction and calculates the derivative using the cubic polynomial drawn through the four involved points. The approximation to surface and volume integrals in eqn (24) generates algebraic system of equations for control volume as –

$$A_p\phi_p + \sum_l A_l\phi_l = Q_p \quad \text{which in matrix form are represented as} \tag{25}$$

$$[A] \bullet [\phi] = [Q] \tag{26}$$

Where [A] is sparse matrix and the coefficient matrix values are updated which depends upon boundary conditions and initial guess and above equality will not hold. The imbalance called residual R defined as -

$$R_p = A_p \varphi_p + \sum_l A_l \phi_l - Q_p \tag{27}$$

Will reduce over the increase in iteration is called convergence. The target value for Root Mean Square - RMS or maximum RMS of the order 1.0e-04 is generally used for convergence criteria based on discretization schemes used for flow equations. Acceleration of convergence also depends on the scheme of matrix inversion techniques employed. It may be noted that level maximum RMS error are always lower than RMS errors and it will take more execution time.

6. Particulate laden flows – erosive wear by particle impacts

Many engineering problems involves the study of multiphase flow mixtures with the combination of gas-solid, liquid-solid phases and its effects were extensively reviewed by Humphrey JAC (1990). Prediction of flows with dispersed phase involves the separate calculation of each phase with source terms to account the interaction between two phases. The flow of the continuous phase is predicted using a discretized form of the Navier Stoke's equations. The particles motion as a function flow velocities/temperatures are predicted using the discrete approach, wherein each individual particle is treated on Lagrangian scale. The most widely applied method available to determine the behavior of the dispersed phase is to track several individual particles through the flow field. Acceleration of particle in the flowing fluid under the assumptions a) Particle/particle interactions are not included in the model. b) Particle interactions may be important in flows, where the discrete phase volumetric concentration is greater than 1% c) there are no particle source terms to the turbulence equations, and therefore turbulence is not modulated by the discrete phase and d) Only inert, spherical particles are considered, are described mathematically as--

$$m_p \frac{dv_p}{dt} = 3\pi\mu d C d\left(v_f - v_p\right) + \frac{\pi d^3 \rho_f}{6}\frac{dv_f}{dt} + \int_{t_0}^{t} \frac{\pi d^3 \rho_f}{12}\left(\frac{dv_f}{dt} - \frac{dv_p}{dt}\right) + F_e \tag{28}$$

$$\frac{3}{2} d^2 \sqrt{\pi \rho_f \mu} \int_{t_0}^{t} \frac{\frac{dv_f}{dt} - \frac{dv_p}{dt}}{\sqrt{t - t'}} dt' - \frac{\pi d^3}{6}\left(\rho_p - \rho_f\right)\omega \times \left(\omega \times \overline{R}\right) - \frac{\pi d^3 \rho_p}{3}\omega \times v_p$$

Detailed derivation of for acceleration of particle and its simplification was discussed by Routhiainen, P.O (1970). The terms on the left-hand side is acceleration of particle motion is the summation of all forces acting on it describes in above equation. The first term indicates viscous drag of fluid over the particle surface according to Stokes law. The second term is the force applied on the particle due to the pressure gradient in the fluid surrounding the particle caused by fluid acceleration. The third term is the force to accelerate the virtual mass of the fluid in the volume occupied by the particle. This term is important, when the displaced fluid mass exceeds the particle mass, such as in the motion of bubbles. The fourth term is an external force which may directly affect the particle such as gravity or an electric field. The fifth term is the Basset force or history term, which accounts for the deviation in

flow pattern from steady state. This term increases the instantaneous flow resistance, when the particle is accelerated at a high rate by an external force and can be significant only when the fluid density is equal or exceeds the particle density. The last two terms are the centrifugal and coriolis forces, present only in a rotating frame of reference. In the eqn (28) third and fifth terms are insignificant, as particle density is higher than fluid density. As a result, the eqn (28) further reduces to

$$\frac{\pi d^3 \rho_p}{6}\frac{dv_p}{dt} = 3\pi\mu d Cd\left(v_f - v_p\right) + F_e - \frac{\pi d^3}{6}\left(\rho_p - \rho_f\right)\omega\times\left(\omega\times\vec{R}\right) - \frac{\pi d^3 \rho_p}{3}\omega\times v_p \tag{29}$$

The drag coefficient *Cd is* obtained experimentally based on size and Reynolds' number of particle. The calculation of the instantaneous fluid velocity, v_f, depends on the flow regime and the type of particle tracking desired. In laminar flows or in flows, where mean particle tracking is calculated, v_f is equal to the mean local fluid velocity, $\bar{v}_f$ surrounding the particle. Prediction of particle motion requires an accurate estimation of turbulent behavior and velocity fluctuations. Turbulent flows consist cascade of eddies, which transport and dissipate the energy. These eddies have a spectrum of characteristic sizes and life times. A particle travelling through a turbulent flow would be exposed to this entire spectrum of eddies, interacting with each for some characteristic time or distance. The particle trajectory calculations are carried out through numerical integration of eqn (29) in the flow filed upto the point of impact. When the particles are flowing through the fluid, its conditions at various locations are defined as follows:

Boundary condition	Action
wall	escapes the domain, reflects, collects, reacts
symmetry plane	reflects
inlet	escapes the domain
outlet	escapes the domain
periodic	particle translated and velocity rotated
grid embedding interface	search for new flux element

The magnitude and direction of the impact velocity relative to the wall surface, for a large number of particles constitute the essential data for the evaluation of erosive wear. To this effect the velocity of a rebounding particle is calculated using the restitution coefficients, which are measured by experiments. When the particle impact/rebound from the wall surfaces, normal/tangential velocity before/after impact of the wall relating to coefficients of restitution, are calculated by using following relations:

$$V_{2t}=e_t V_{1t} \tag{30}$$

$$V_{2n}=e_n V_{1n}$$

The restitution ratios are determined experimentally based on flow velocity, particle and target material. The coefficient restitutions are calculated using

$$e_t = 1 - 2.12\beta_1 + 3.0775\beta_1^2 + 1.1\beta_1^3 \tag{31}$$

$$e_n = 1.0 - 0.4159\beta_1 + 0.49943\beta_1^2 - 0.293\beta_1^3 \tag{32}$$

Where β is impact angle in radian. With the values of coefficient restitution, impact angle and velocity, the erosive wear can be estimated with the following relation:

$$E = AV\beta \tag{33}$$

User need to specify the inputs for particle resident times, coefficient of restitution, particle material, density etc to calculate erosive wear by particle impacts. In turbo machinery applications, these particles under two phase flow conditions, experience different degrees of turning, as they flow through blade channels. The damage due to particle impacts are manifested by pitting and cutting of the blade leading and trailing edges are compressively discussed by Tabbakoff (1983). The overall effect of the phenomena from the aerodynamic point of view is an increase in total pressure loss across the blade row. However, the particulate laden flow simulation and its effect in the recyclic cyclone used in power generation are discussed at length under the case study-3.

7. Structural deformations due to flow pressure loads – FSI

The mathematical formulations to simulate structural deformations and stresses on the component surfaces are extensively discussed by Mustafa (2006). To determine the deformations, governing equations are mathematically represented as –

$$\rho\ddot{u} = \nabla \bullet \sigma + b \tag{34}$$

Where $\ddot{u}$ is displacement, σ is stress field depends on strain, internal variable, b – body force. the expression for strain in terms of displacement can be expressed as

$$\bar{\varepsilon} = \frac{1}{2}\left(\nabla\ddot{u} + \nabla\ddot{u}^T\right) \tag{35}$$

The finite volume form and after integration by parts, the eqn (34) can be written as

$$\int_V \rho\ddot{u}dV = \int_A \sigma\, ds + \int_V bdV \tag{36}$$

For all cells i in the domain V, the discrete form of the momentum equation becomes:

$$\rho_i\ddot{u}_iV_i = \sum_{j\in f(i)} f_j + b_iV_i \quad where \quad f_j = \sigma_j \bullet s_j; \quad s - surface\ vector \tag{37}$$

Dropping intertial terms and considering some of the forces acting on the body is zero for a static case, the eqn (37) can be re-written as –

$$r_j = \sum_{j\in f(i)} f_j + b_iV_i \tag{38}$$

In order to compute the stress tensor $\bar{\varepsilon}$ on the centroids of the faces, it is required to establish the discrete form of the strain tensor and the deformation gradient $\nabla\ddot{u}$. The deformation gradient is computed at cell centers based on the difference in displacement between neighboring points. The approximation of stiffness matrix can be accumulated over all faces are –

$$K_{ik} = -\frac{\partial r_i}{\partial u_k} = -\sum_{j \in f(i)} \frac{\partial f_j}{\partial u_k} \quad \forall_{i,k} \in N(i) \tag{39}$$

With the help of Newton method to correct displacement Eqn (38) further simplifies to

$$K_{i,k} \nabla \ddot{u}_k = r_i^n \quad ; \quad \nabla \ddot{u}_k = \ddot{u}_k^{n+1} - \ddot{u}_k^n \tag{40}$$

To obtain structural deformations, pressure/heat flux loads are normally obtained from CFD solver using finite volume approximations and deformations/stresses are obtained through finite element techniques. However, in the current versions of few flow solvers, flow and thermal stress based on finite volume techniques can provide FSI characteristics of industrial components. A detailed discussion of a case related to transition duct used in gas-turbine application is presented under the case study-4.

8. Pressure waves – generation of aerodynamic noise

Aerodynamic noise results from the propagation of disturbances through the fluid flows at some point in time and space. Whether the disturbance is caused by an object or the fluid itself, fluctuations in fluid pressure propagate outwards from the source at the speed of sound relative to the fluid. Theory associated to noise as function of flow pressure was discussed by Alan Powel (1994) and the size of the pressure fluctuation relative to the pressure is called the sound pressure level. The sound intensity $\boldsymbol{I}$ defined as -

$$I = \frac{p'}{2\rho c} \tag{41}$$

where p′ is fluctuating pressure, ρ - density of fluid and c - is speed of sound. Pressure and velocity fluctuations are simulated from CFD simulations in the near field noise. The near field will likely include the locations, where the maximum noise levels occur. For most CFD simulations the extent of the computational domain is usually such that near field/far field noise can be estimated.

The near field pressure and velocity fluctuations play a key role in determining far field noise, which occurs at some distance by acting as a localized source of noise. The influence of turbulence modeling on the broad band noise simulation for complex flow simulation by Greshchner (2004) has provided valuable insights to predict overall sound pressure and power for an application to rod-aerofoil. In many practical applications involving turbulent flows, noise does not have any distinct tones, and the sound energy is continuously distributed over a broad range of frequencies. Assuming that the fluid is a perfect gas, homogeneous wave equation is solved using noise sources taken from CFD are defined as –

$$\frac{\partial^2 \rho'}{\partial t^2} - c^2 \frac{\partial^2 \rho'}{\partial x_i^2} = \frac{\partial^2 \overline{T_{i,j}}}{\partial x_i \partial x_j} \tag{42}$$

Where $\overline{T}$ is Lighthills tensor, ρ′ is density fluctuation with respect to ambient condition. It assumes that the ambient fluid is an isothermal polytrophic gas so that the pressure fluctuation is directly proportional to the density fluctuation. As a result, the eqn (42) can be

written in terms of either pressure or density variation. The Lighthill tensor has three components defined as

$$\overline{T}_{i,j} = \rho\, u_i\, u_j \quad + \quad p_{i,j} \quad - \quad c^2 \rho' \delta_{i,j} \tag{43}$$

Where the first term Reynolds stresses and $p_{i,j}$ is the stress tensor. One approach is to solve Lighthill equation to predict the noise source strength on a separate acoustic mesh, which is normally much coarser than CFD mesh. This approach significantly reduces the cost of solving for the far field noise using turbulent compressible Navier Stoke's equations, accounting the effects like reflections, diffraction or absorption besides frequency analysis. The noise sources present due to turbulent flows shown in Fig-11 are extensively discussed by Sandeep Sovan (2005)

In terms of noise sources, the eqn (42-43) can be re-rewritten as –

$$\frac{\partial^2 \rho'}{\partial t^2} - c^2 \frac{\partial^2 \rho'}{\partial x_i^2} = \frac{\partial}{\partial t}\left\{\rho_0 v_n \delta(f)\right\} - \frac{\partial}{\partial x_i}\left\{p_{i,j}\delta(f)\right\} + \frac{\partial^2 \overline{T}}{\partial x_i \partial x_j} \tag{44}$$

Where $\delta(f)$ describes the source of geometry, v_n normal velocity and $p_{i,j}$ stress tensor is given by

$$p_{i,j} = p\delta_{i,j} - \mu_{eff}\left(\frac{\partial u_i}{\partial x_j} + \frac{\partial u_j}{\partial x_i}\right) - \frac{2}{3}\mu_{eff}\frac{\partial u_k}{\partial x_k}\delta_{i,j} \tag{45}$$

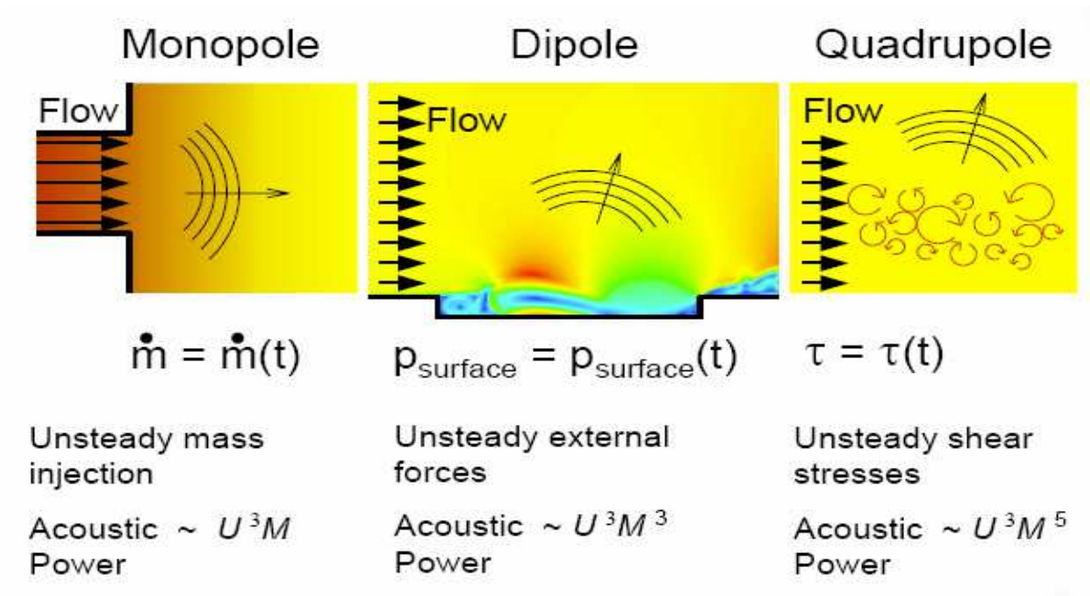


Fig. 11. Illustration of aerodynamic noise sources

In the right hand side of the eqn (45), first, second and third terms indicates mono/dipole/quadro poles noise sources respectively. The eqns (44-45) are called aero acoustic formulation by Ffowcs Williams and Hawkins. In CFD software, the noise resulting from unsteady pressure fluctuations can be computed in several ways. Transient LES

predictions for surface pressure can be converted to a frequency spectrum using the built-in Fast Fourier transform (FFT) tool in most of the flow solvers. The Ffowcs Williams–Hawkings acoustics whose derivation was extensively discussed by Ffowcs W J E and Hawkings D L (1969) are used to model the propagation of acoustic sources for objects ranging from exposed bluff bodies to rotating fan blades. Broadband noise source models allow acoustic sources to be estimated based on the results of steady-state simulations provides practical tools for interpretations of noise sources. More comprehensive analysis for predicting sound directivity, reflections and radiations can be analyzed through CFD commercial software like CFX, Fluent and Star-CD even though simulation needs special purpose commercial software like Sysnoise/Actron for comprehensive investigations for far field noise. The typical simulation has attempted to compute different noise source strengths and frequency analysis for an axial fan using RANS equations are discussed under case study-5.

9. Flow simulation in coal pulveriser – case study: 1

Fuel preparation for the boilers through grinding the coal has been made in the pulverizers. The grinding mills can be different types like ball, impact and the roller mill is also called bowl mill is extensively used in Indian coal fired power station. The need to design more efficient grinding elements are necessary to increase thermal efficiency of boiler auxiliaries. If the coal fails to burn as required, the alternatives available to pulverize operators are limited and results in combustion inefficiency in the boiler, was reported in the technical paper by Mechthild Angleys et.al (1998). The Electric Power Research Institute has reported that 1% of plant availability is lost on average due to malfunctioning of pulverizer internals.

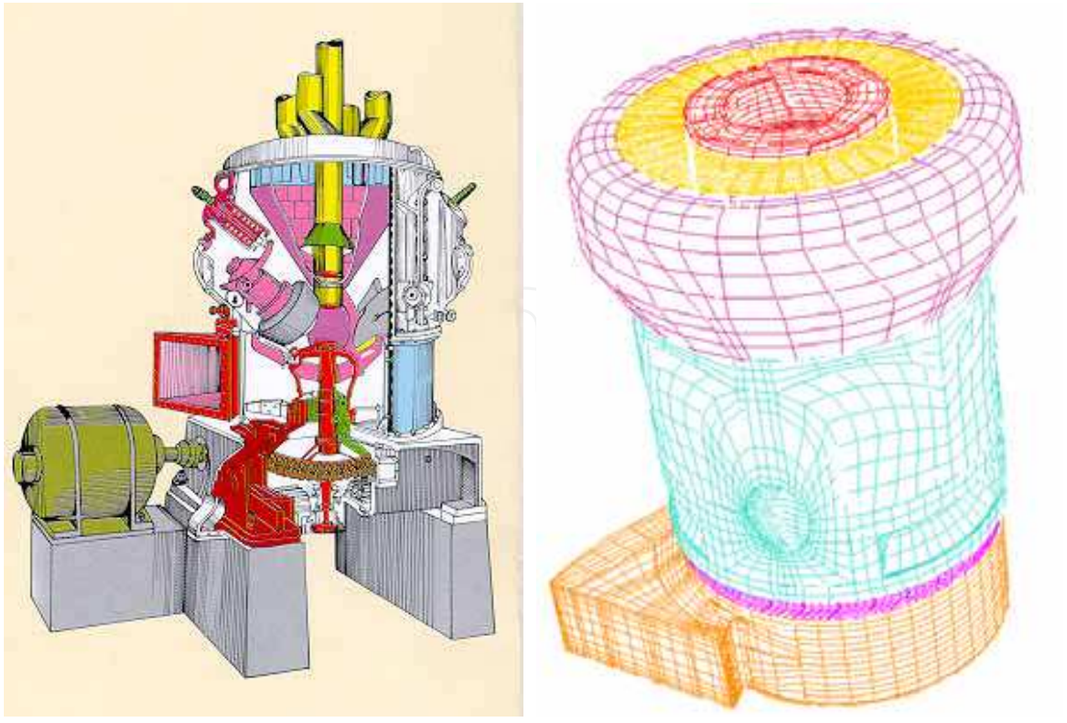


Fig. 12. (a) Isometric view of the mill (b) Computational grid

To understand the flow pattern inside the different types of pulverizers, numerical simulations were described by Mechthild Angleys (1998) and CAJ Fletcher (1993). Based on these works, CFD analysis in the roller mill was discussed by C.Bhasker (2001) whose isometric view in three dimensions are shown in Fig-12(a). This mill is used to separate coal particles based on centrifugal forces due to spinning motion of bowl. However, due to bowl rotation, particles are moved away to clearance, where rollers crush them into fine powder with the pressure forces by the springs attached to it. The air flow enters tangentially through inlet duct vanes lift these particles towards classifier vanes and exit pipes connected to boiler. The coarse particles, which are not separated will fall back to bowl for re-grinding. Flow around different internals present inside the pulverizer is complex and are prone to secondary and tertiary swirl motion.

The flow travels in the mill around stationary and rotating internals crosses bowl rim, rollers, vanes at inlet, classifier vanes and exit coal outlets have geometrical complexities involving steep curvatures and steps. CAD modeling from the assembly of manufacturing drawings with all internals has been carried out and extracted the flow passage. The flow passage around the solid objects is further decomposed to generate high quality structured computational meshes in different parts. The computational mesh shown in Fig-12(b) in different parts are imported in the flow solver for flow simulation. The grid-interfaces between parts of the meshes are created to remove duplicate elements at mating surfaces. The computational mesh of 120,000 point data has been generated in 307 grid blocks with several connections between blocks to avoid the prevention of flow due to presence of artificial walls. The CFD software TASCflow from AEA Technology/Canada based on finite volume method has been employed to solve 3-dimensional RANS equations for incompressible flow. Turbulent effects are accounted through k-ε model with standard wall functions. The mass flow of 29.6 kg/s is assumed to be entering in the pulverizer through inlet fixed with five vanes and leaves through exit locations, at which static pressure of order 6.16 ata has been specified for flow simulation.

The convergence of equation residuals for simulation of flow in the pulverizer along its internals depends on proper initial guess and under-relaxation factors. The optimum value of time step, which is based on trial and error method was provided to accelerate the convergence for flow simulation. Besides time step, dropping of error in the equation residuals also requires proper inputs for turbulence intensity and length scales at inlet location. With suitable initial guess values for flow momentum, pressure and turbulence quantities and under-relaxation factors in control parameters, the simulation took about 300 iterations for completion of flow simulation on 256 MB RAM Compaq Pentium-III 450 MHz work station. After completion of simulation, with the help of result files, several planes across the mill height and horizontal directions are created from the grid block nodes using region manager available in solver post processor. The flow visualization in terms of velocity vectors/contours different cross-section of device and streak lines from the inlet of mill chamber are generated to understand the flow distribution. The velocity vectors in the planes over the height of the mill are described in Fig-13(a) wherein the flow path is highly non-uniform and exhibits recirculating flow especially in the inlet region. As a result, flow in the mill exit locations are leaving with unequal velocity as seen in Fig -13(b). The air flow in terms streak lines drawn from the inlet of mill indicates that its paths are not reaching to classifier with required intensities due to flow recirculation observed at several locations in the mill. The observations from the simulation have shown significant impact on existing designs for improving the flow distribution by small changes in the geometries.

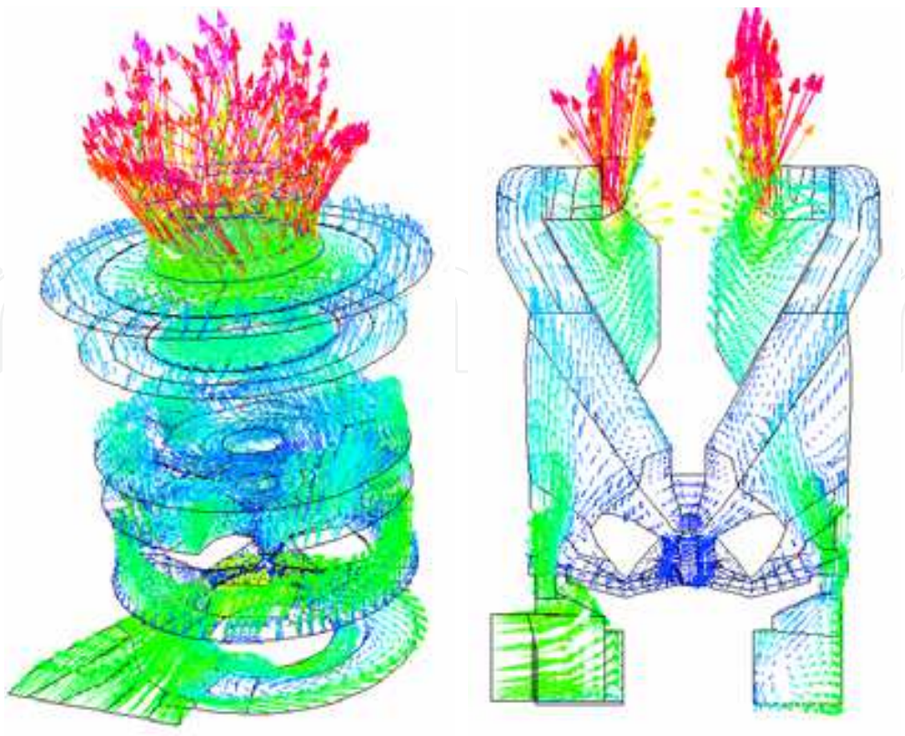


Fig. 13. Velocity vectors in the mill (a) over height [b) horizontal plane

9.1 Flow analysis in electrostatic preceiptator – case study: 2

Electrostatic precipitators are extensively used to collect particulate emissions from the power production units. Although the performance of the precipitators are high, their collection efficiency is strongly dependent on the electro hydrodynamic behavior of two-phase flow inside the chamber. The problems faced in the operation of ESPs depend on many factors such as gas volume, particle size distribution, gas-temperature, mechanical conditions, etc., Indian coals have high ash content, can effect electrical resistivity and particle size distribution besides disturbing uniform flow pattern, as discussed by Srinivasan (1996).

The gas velocity characteristics with an electrostatic precipitator play an important role in overall ESP performance. If local gas velocities are too high, then the aerodynamic factors depends upon the particles can overwhelm the electrostatic forces generated by the collecting surfaces and electrodes. This leads to degradation in collection efficiency and techniques to improve its performance was outlined in the paper by Dumont (2001). If the local velocities are too low, the collecting surfaces are not being utilized and the potential of particulate deposition. In view of these problems, proper design of flow control devices within ESPs are critical. Construction of physical model includes turning vanes, baffles and perforated plates in several combinations are complex task for development of ESP. The analysis of ESP flow characteristics through physical scale model was only the choice until now are expensive and time consuming process, as the change in configuration will limit to use of existing models.

Many CFD studies as an alternative have been made to understand the flow distribution in ESP especially using skew gas flow technologies by Schmitz (2001). The multi-disciplinary

flow simulation influencing the flow distribution towards emitting electrode by Gallimberti (1998) and Varonos (2002) are the major contributions for improving the efficiency. However, still there is a need to understand the following parameters, which influences performance degradation in ESP.

- Resistivity
- Ash quality
- Ash distribution
- Gas composition
- Gas temperature
- Gas distribution
- Duct geometry
- Inlet geometry
- Electro-static forces
- Electrode geometry
- Collection plate geometry
- Rapping

Depending upon power station rating, the configuration of ESP varies in terms of fields and length, height, width of chambers. The ESP chamber also can be single or multiple pass connecting to one or two chimneys varies based on power plant layout. The entrainment of flue gases in the ESP chamber from the air-preheater is subjected to several internals like inlet funnels, gas distribution screens, outlet funnels and induced draft fans to stack. The prediction of uniform flow from the air-pre heater to ESP chamber through several flow control devices placed in the ducts, splitter vanes, gas distribution screens involves complicated process, as modeling the gas distribution screens placed in the ESP inlet and exit location will an important issue.

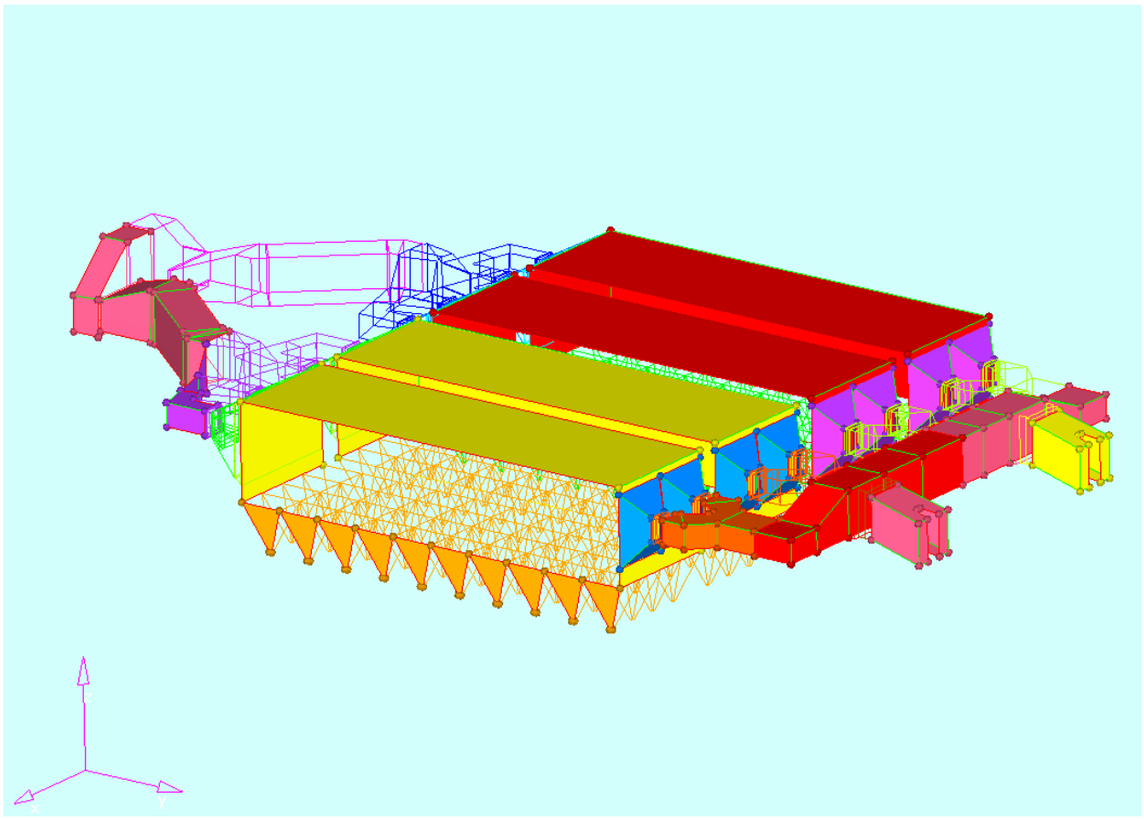


Fig. 14. Isometric view of four pass ten field ESP configuration

As suggested by Nielsen (2001) gas distribution screens are simulated by two different methods a) that of porous baffle computational cells, which are effectively zero thickness

may be placed between any two fluid cells b) use of source term model which requires experimental input. Both the models implement the forces from the screens acting on the flow without modeling the geometrical details of the screens. Accurate modeling of the gas distribution screen geometries comprises several thousands of holes are time consuming process with even large and fast computers. To overcome this, the momentum equations with the lift and drag sources are introduced, wherein its coefficients depends on angle of attack and screen design. Using above approaches, flow through four fields single pass ESP as part of retrofit for the power producing unit was analyzed by Bhasker (2005) and estimated the pressure drop across this cleaning device. This work has renewed the interest to know the flow uniformity at inlet duct outlet of higher rating ESP, whose isometric view is shown in Fig: 14.

In order to study the flow distribution in the inlet duct portion of four pass two ESP configuration connected to two ID fans, IGES file from CAD model has been imported in CFD pre-processor. The geometry of inlet duct with flow control devices shown in Fig-15(a) is considered to develop the flow pattern inside the duct around flow control devices. Accordingly the computational domain was discretized into number of blocks past the turning vanes present in the duct. The computational domain is divided through number of blocks in such way that grid points are captured on turning vane surfaces. In the process at several places, triangular shape portion forms in the domain and computational mesh from upstream blocks disturbs element node connectivity. To over come this, triangular shape blocks present in the domain are further divided into Y type blocks to make uniform topological connections between grid blocks. After checking the edges discontinuity between grid blocks in the computational domain using solid mesh options available in grid generator, mesh has been filled firstly in smallest volume. In order to ensure topological connection between grid points in neighboring volumes, hex elements are filled in the smallest block while varying the node distribution in flow direction. The computational grid for the ESP inlet duct with turning vanes comprises 445071 nodes generated is shown in Fig-15(b). After generation of grids, duplicate elements are removed through check edge option, adjusting the default tolerance values. Software has several other quality checks especially Jacobeans and face checks. Any negative Jacobeans will indicate distortion of elements leads to negative volumes and such grid data cannot be accepted by flow solvers. Face check indicates computational grid inside the flow volume is free from duplicate/distorted elements. Using this face grid collector, several boundary conditions regions are created and exported to several flow solvers like, TASCflow, Fluent, CFX and Star-CD for benchmarking the simulation.

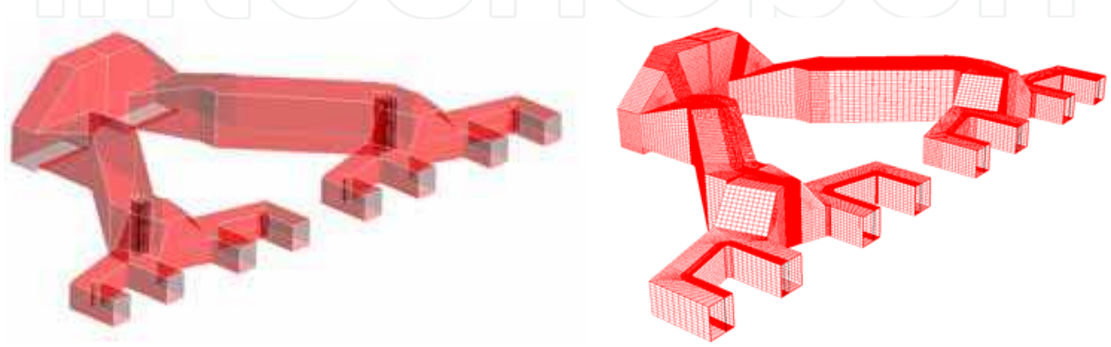


Fig. 15. ESP Duct (a) Geometry (b) Computational Mesh

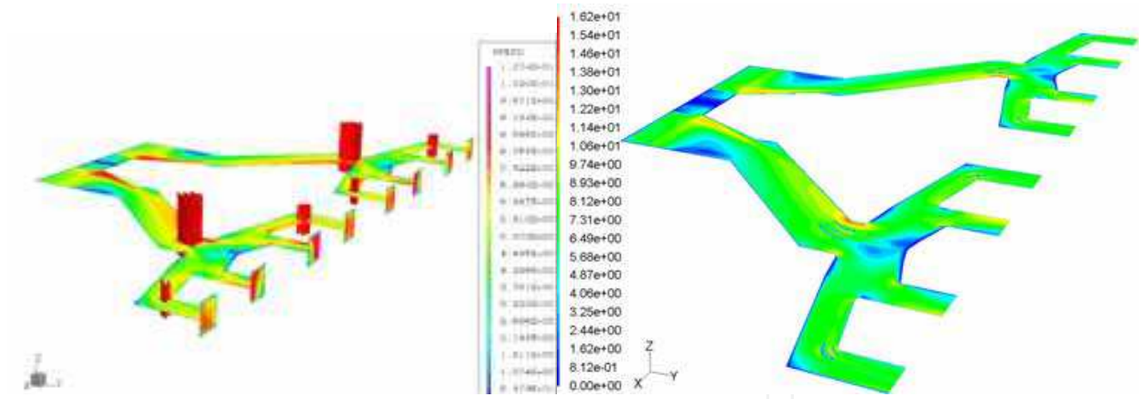


Fig. 16. Velocity in the middle plane a) TASCflow b) Fluent flow solvers

The flow pattern in the middle plane of the duct using TASCflow and Fluent solvers is shown in Fig-16(a-b). It is observed that flow separation in the case of fluent solver is better than the same obtained using TASCflow solver. However, CFX and Star-CD solvers comprises robust multi-grid algorithms along with advanced post-processing features provides excellent visualizations and estimation of averaged flow quantities at duct outlet. The velocity pattern in form of streamlines are better predicted separation regions near corners using CFX and Star-CD. All the solvers have predicted that that flow at eight ducts outlet are not uniform and required to be improved by adding more flow control devices. This bench mark study with more details available in the paper by C.Bhsker (2011) also reveals that fluent-3D can be best choice for feel of results quickly. CFX and Fluent along with several pre/post processors all merged with Ansys are available under current version through workbench to study multi-disciplinary simulations including fluid-solid interactions even with electro fluid dynamic effects. The Cd-Adapco's current version or star-ccm solver with similar features provides another alternative on polyhedral cells for flow visualization and quantification of results. The cross comparison presented in this work proves that the basic numerical techniques through multiple flow solvers are reliable and deliver the expected performance in terms of accuracy and convergence.

9.2 Particulate laden flows in cyclone collector – case study: 3

The cross sectional view of cyclone separator along with other components used in Circulating Fluidized Bed Combustion - CFBC plant for supply of electricity to paper manufacturing unit is shown in Fig-17. Flue gas produced out of the solids used in the combustor enters to refractory lined cyclone. The cyclone collects more than 99% of the incoming solids, which travel down the conical bottom to the sealpot blower and are eventually siphoned back into the combustor as detailed by Rajaram (1999).

The flue gas leaves the cyclone top flows on to a convective pass containing three stages of super-heater and economizer. A tubular air heater forms the last heat recovery surface and preheats the primary/secondary air streams separately with the air flowing inside the tubes and gas flowing outside them. The flue gas is then enters in an electrostatic precipitator and leaves towards stack through induced draft fans. Although the operation of the plant with varied load is successful, there were problems related to flue gases, which are coming from the cyclone outlet are settling on the super-heater tubes, concern the plant efficiency.

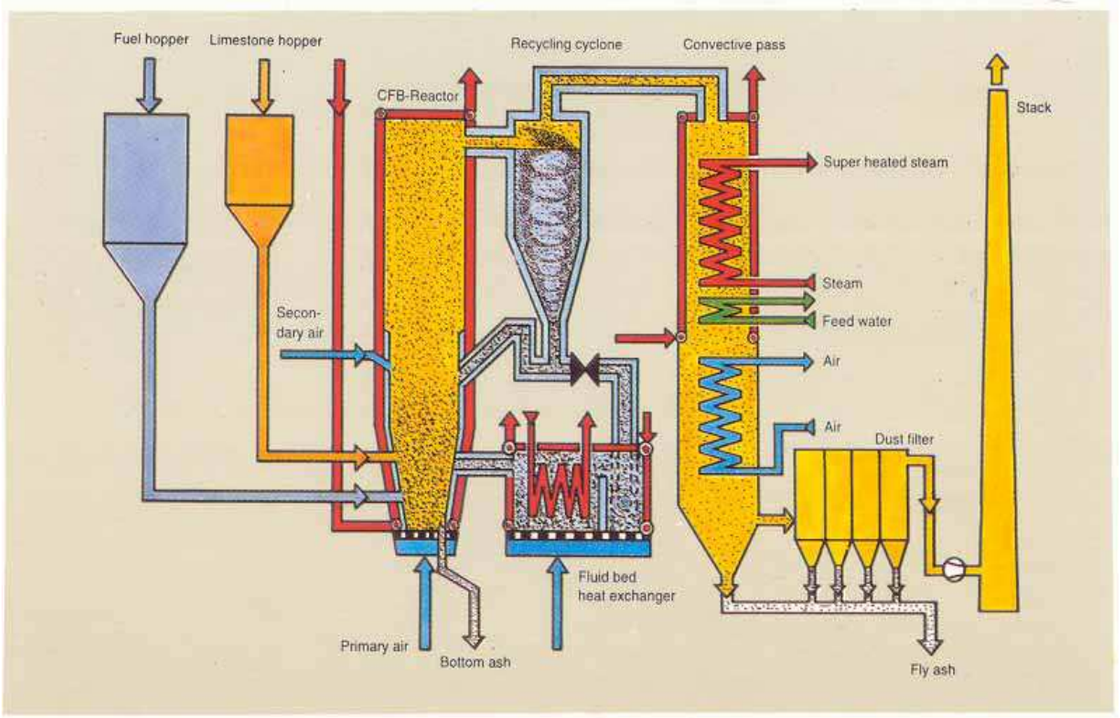


Fig. 17. Location of Recycle cyclone in CFBC power plant

The flow in cyclone separator is highly turbulent due to swirl motion and several investigations are carried out by Slack (2000) and Fraser (1997) using advanced numerical techniques. The geometry of cyclone separator used in paper manufacturing industry considered for flow and particle trajectories are different from the conventional cyclone separator, as it is placed between boiler and tube banks of power plant. However, its basic geometry resembles with conventional one, the orientation of inlet and exit duct attached to it are different. The cyclone collector considered consists of an upper cylindrical part, with a tangential inlet and lower part with an exit at the apex. They are used to separate dispersed heavy substance from a fluid of lower density, the suspension to be separated being injected with high velocity tangentially into the cyclone. These results in high spin velocities within the cyclone, which produce a large centrifugal force field. The separated material leaves the cyclone at its apex, while clean fluid is discharged at the top through the overflow pipe.

The geometrical model of cyclone has been created from assembly drawing using CAD modeler I-DEAS and its output is exported to CFD pre-processor for extraction of flow passage. ICEM CFD pre-processer has flexible tools for mesh generation with several surface repair options. In order to proceed for mesh generation, initialized block is placed on the computational domain and the same has been divided through horizontal and vertical directions using splitting options, according to geometry shape and internals. The resulting block edges are aligned to geometrical edges using project/associate commands. With this referenced block, using its face selection, topologically connected blocks are constructed for rest of the geometrical part. To obtain the computational mesh in three dimensions, nodes to master linking to slave edges are to be specified. Software provides several distribution laws for clustering the nodes on boundary surfaces. The pre-view of the nodes on the master and

slave edges with direction arrows provides the first insight for the proper mesh distribution on the geometrical part. The activation of volume mesh, under mesh generation option provides three dimensional meshes for the specified solver format. After completion of mesh generation in different parts, the assembled mesh has been imported in flow solver is shown in the Fig-18(a) with grid interfaces between parts so that no artificial walls present in the volume grid.

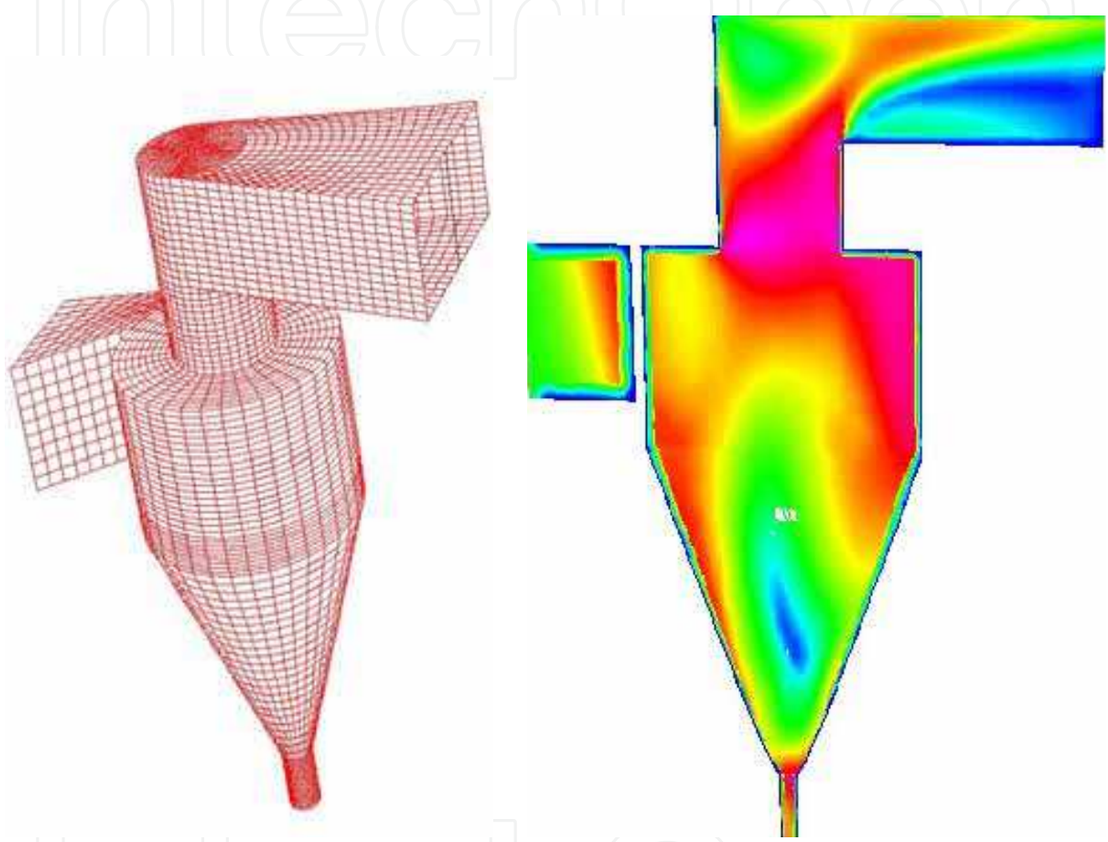


Fig. 18. Cyclone Collector (a) Computational Mesh b) Velocity Contours

After description of fluid properties in flow solver, boundary conditions for the velocity and pressure are prescribed at inlet and exit locations. In order to capture the viscous effects, two equation turbulence model based on intensity and length scale with standard wall functions are employed. Since the flow inside the cyclone collector is highly rotational and the option of covariant velocity in normal direction has been used as an initial guess for flow simulation. From the simulation results it is observed that the velocity distribution from inlet of cyclone leaves through one side of the outlet duct indicating that flue gas comprises particles settles on super heater tube bank surfaces. Simulation of flow in the existing configuration of cyclone separator also indicates that particles are unable to reach with required velocity magnitude in the outlet duct region due to large flow recirculation.

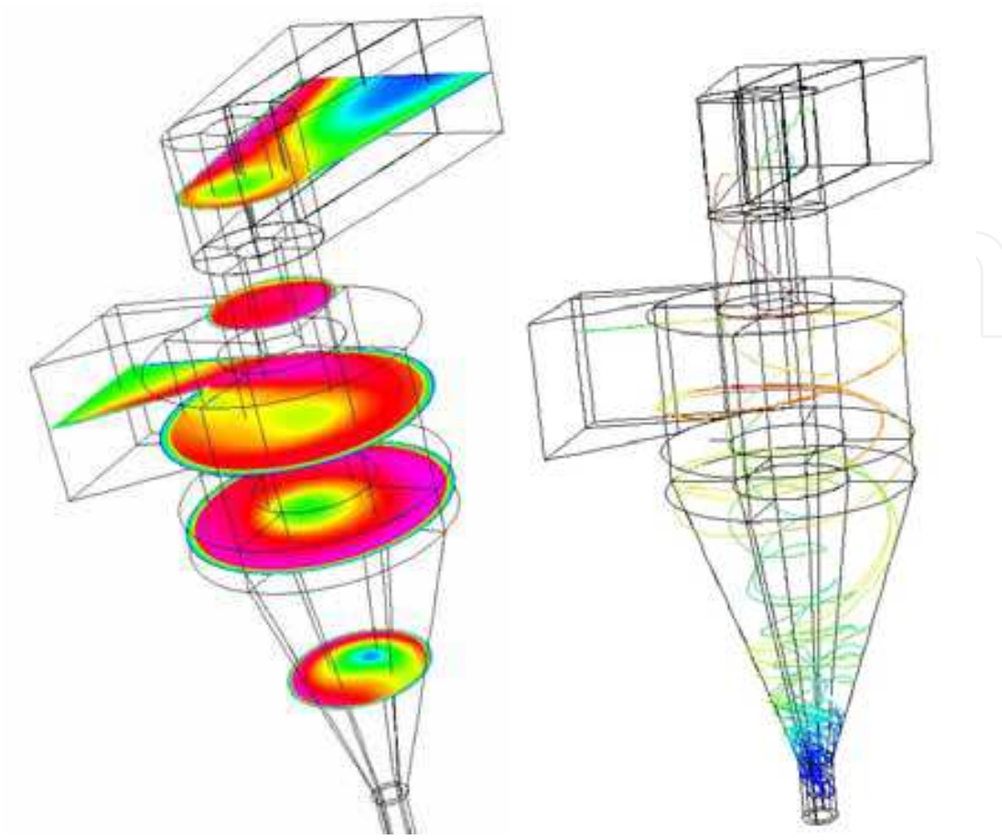


Fig. 19. Improved geometry (a) Velocity pattern b) Particle trajectories

To improve the velocity distribution, geometrical changes with two baffle plates in the outlet duct of the cyclone separator are provided in the CAD model. Multi-block hexahedral element mesh has been re-generated and imported in the flow solver. After obtaining successful flow simulation, discrete phase of particulate media has been added to working fluid to track the particle trajectories in the cyclone collector. The inputs like particle resident times, particle material and particle sizes according to distribution laws are defined for two-phase gas-solid particle flow simulation. The velocity contour plots over height of the modified cyclone separator is shown in the Fig-19 (a), wherein it is noticed that presence of partition plates reduces the flow recirculation in the outlet duct and thus decreases the settling of particles on super heater tubes. From the particle trajectories plot Fig-19(b), it is observed that the particle size 10 microns follows air flow along the wall of vortex tube finder to gas exit. Bigger size particle of 100 micron released from the inlet of cyclone separator moves along the outer conical wall. This is because the particles have low inertia and associated drag force decelerates the fluid motion. It also follows the recirculation gas flow back into the cyclone body, where it is captured into the vortex core and moves upward to the outlet gas. The larger particle of 1000 micron size captured in a particle rope and later follows the recirculating flow to the vortex finder and separated from the fluid stream towards cyclone bottom outlet. The detailed simulation of flow in cyclone collector with formulations are comprehensively discussed in the paper by C.Bhasker (2010).

9.3 FSI studies on gas-turbine transition duct – case study: 4

In order to achieve higher net power outputs and thermal efficiencies, turbine inlet temperatures (TITs) have to be as high as possible in compliance with technological limits. As a consequence, hot gas path parts (HGPPs) are exposed to severe thermal conditions leading to high metal temperature, which are responsible for the deterioration of hot gas carrying parts. They include all components associated with the combustion process liners, fuel nozzles, transition pieces, buckets, shrouds, etc. In a gas turbine combustion chamber, the transition piece carries the hot gases from its outlet to turbine first stage, as shown in Figs 20(a-b) to the turbine.

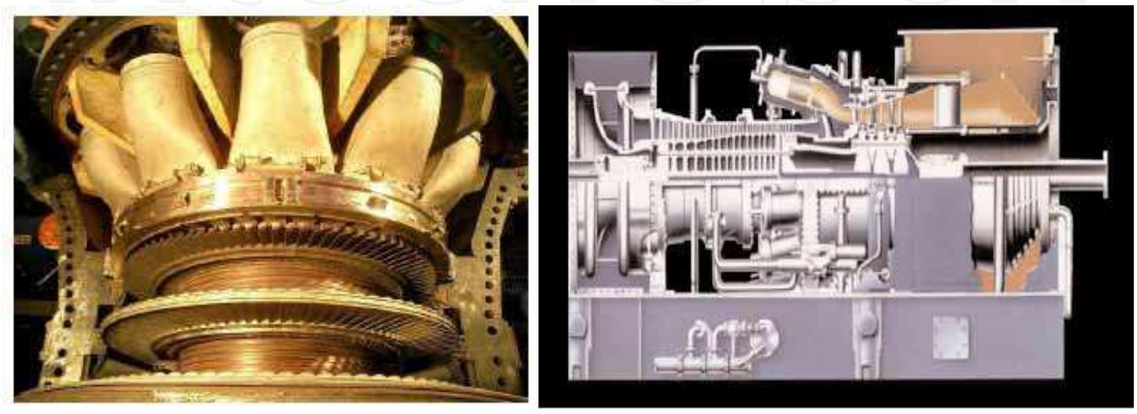


Fig. 20. (a) Transition Duct (b) Location of Transition duct in Gas-Turbine

The gas turbine field engineering team has reported that unscheduled engine outages can occur as a result of premature part failure in the gas turbine flow path. As a consequence, initiatives were launched to address these fleet-wide combustion and turbine hardware field issues. The efforts were initiated at user request after a large number of 501F machines began exhibiting chronic transition duct failures across the fleet, causing forced outages, which significantly affect the revenue generation as reported in the publication by Jeff Benoit (2007). The duct in which cross sectional shape often follows a circle to rectangular transition with stream wise curvature and combined effects of viscosity/geometry produce a secondary flow in the form of stream wise vortices. These vortices significantly affect the overall performance of the system, for instance, the pressure drop and flow uniformity. Due to presence of steep curvature in stream wise direction, prediction of turbulent structure at near wall region is very critical.

In design context geometric constraints will often dictate the use of possible shortest possible duct for the given cross sectional shapes at inlet and outlet. In this case, the level of separation and severity of flow distortion at the duct exit due to transverse vertical motion are function of aspect/length ratio and cross sectional variation in the transition portion. The design of this duct contains an inlet was subjected to laboratory model for measurements by Davies (1991) later several flow simulations was carried out by Richard Cavicchi H (1999) and Sugiyama H (1999). Based on these investigations, Bhasker (2009) has undertaken comprehensive fluid solid interaction studies on transition duct, which has a sharp transition from circular to rectangular arcs over a short axial and radial distance. The circular to rectangular duct based on inlet dia, exit aspect ratio, length of the transition duct

was constructed. At each stream wise location, the cross-sectional shape is defined by the elliptic equation –

$$\left(\frac{y}{a}\right)^{\eta} + \left(\frac{z}{b}\right)^{\eta} = 1 \tag{46}$$

The parameters a, b and n are functions of stream wise coordinate x. The cross-sectional shape of these transition ducts constructed in six sections becomes more rectangular as the value of the exponent n increases, but they never truly rectangular. In the Fig-21(a), section-1 is inlet diameter upstream of the start of transition (section-2), section-3 and 4 are in the mid-region of transition, section-5 is at the end of transition and section-6 is 2 times of inlet diameters downstream of the duct, with a flanged juncture between station 5 and 6. The ratio of major to minor axis lengths at the duct exit is referred as aspect ratio. For fixed x/D, using the polynomial coefficients for a, b and n, the profile for the duct are generated through a computer program and decomposed into several blocks for computational mesh generation shown in 21(b).

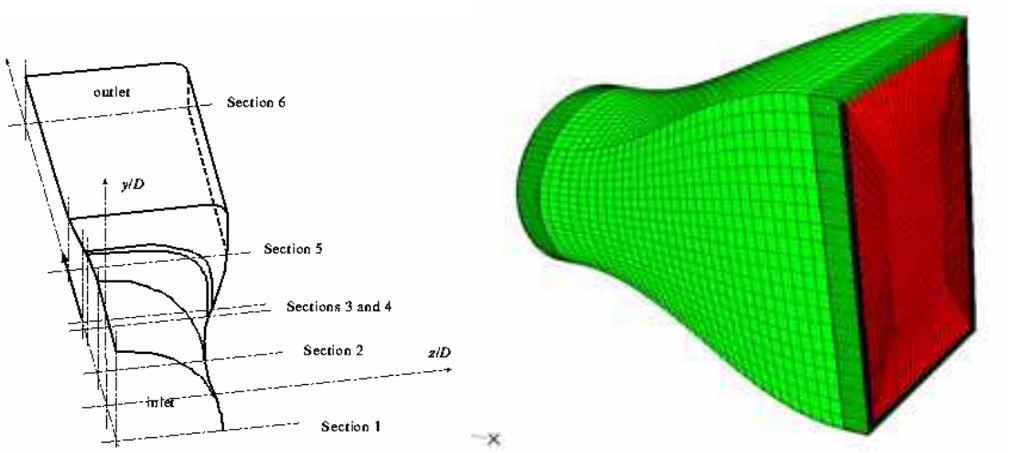


Fig. 21. Transition Duct (a) Geometry b) Computational grid

The grid shown above comprises 127623 nodes along with face grid was created using commercial grid generator. It has been ensured that elements present between block to block at mating surfaces are one-one so that volume grid is free from any artificial walls. Simulations were carried out using commercial flow solver fluent and the flow pattern obtained in the horizontal planes are shown in the Fig-22(a). The velocity magnitude reduces along the stream wise direction towards the duct exit. This is more pronounced in the flow downstream close to exit location. This is because of the flow expansion due to the enlargement of the duct.

Moreover, the deceleration of the flow in the radial direction is more significant close to the outer casing. Consequently, fluid close to outer casing attains lower velocity with turbulent eddies. This is because of the axial momentum is considerably higher than that occurring in the radial direction. The flow in stream wise direction near wall planes at central portion is smooth. In view of secondary flow pattern prevailing in the duct, it is observed that the flow distribution at its exit location exhibits highly non-uniform. Fig-22(b) shows the

pressure distribution on transition duct surface. In general, the wall static pressure is a function of cross sectional area, wall curvature and viscous forces in the flow. Concave curvature along the upper wall induces positive pressure gradient which influences maximum pressure near exit wall surfaces. Conversely convex curvature along the side walls induces negative pressure gradient resulting minimum pressure. Also the radius of curvature of walls at changes signs between stations 3 and 4, which causes maximum and minimum pressure along the side and upper walls respectively. It is also noticed from the figure that undulations exit in the distribution due to vortex flow in close proximity.

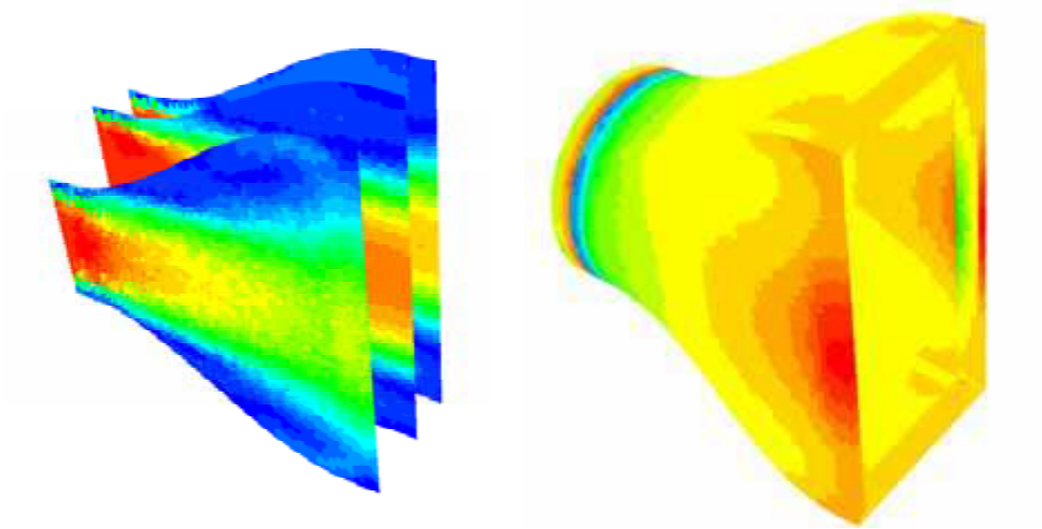


Fig. 22. (a) Velocity in duct planes (b) Pressure on wall surface

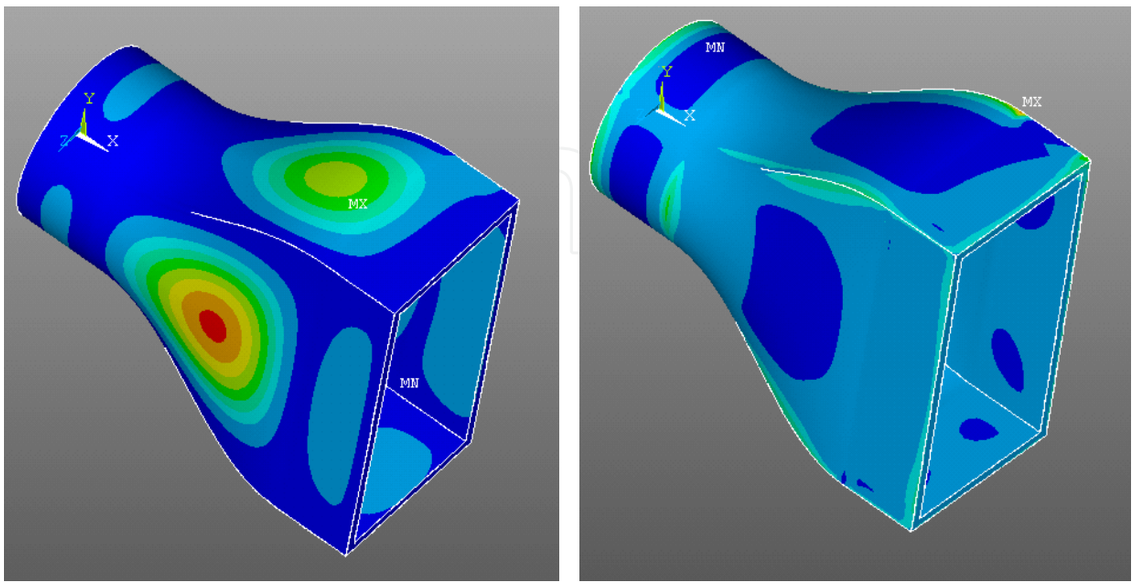


Fig. 23. (a) Displacement (b) Von-Mises Stresses

From the physical point of view fluid structure interactions are a two field problem; one is related to flow simulation, and another is related to structural stress determination. These fields are coupled via the so-called wet surface where the pressure and friction forces caused by the fluid are acting on the structure. Due to these loads the component structure is subjected to deformations and these changes can affect the equivalent stresses.
In order to understand the component deformations due to influence of pressure gradients of transition duct inner profile, static structural analysis has been carried out using the Ansys Mechanical Solver. Computational mesh for transition duct was created using solid element. After specifying material and elastic properties, displacement and pressure loads are transferred from CFD solvers to obtain the displacement and equivalent stresses on the transition duct. The magnitude of maximum displacement is observed in Fig-23(a) at station 4 of transition duct and high stresses are noticed at transition edges as shown in Fig 23(b) are not high enough to produce severe material damages.

9.4 Aerodynamic noise prediction from axial fan – case study: 5

Fans are extensively used to transport the air from one device to other in coal fired power station. Outages of these components due to operational problems are concern the efficiency of critical equipment. Two kinds of fans are normally employed i.e., centrifugal/axial fans; in the former one air accelerates radially outward in a rotor blades in the scroll casing. The fluid is accelerated to parallel to the fan axis in the case of axial fan. Fan performance is best expressed in the form of fan curves between static pressure, horsepower, and efficiency as a function of volumetric flow rate. Axial fans are employed in Induced Draft – ID fans which will have unique characteristics called stall. Stall is the aerodynamic phenomena, which occurs when it is operated beyond its performance limits and flow separation occurs around the blade. If this happens, the fan becomes unstable and no longer operates on its normal performance curve. Extended operation in the stall region should be avoided for excessive noise levels as reported by Subramnian (1984). The poorly designed inlet or a sharp turn just upstream can affect the performance of fan.

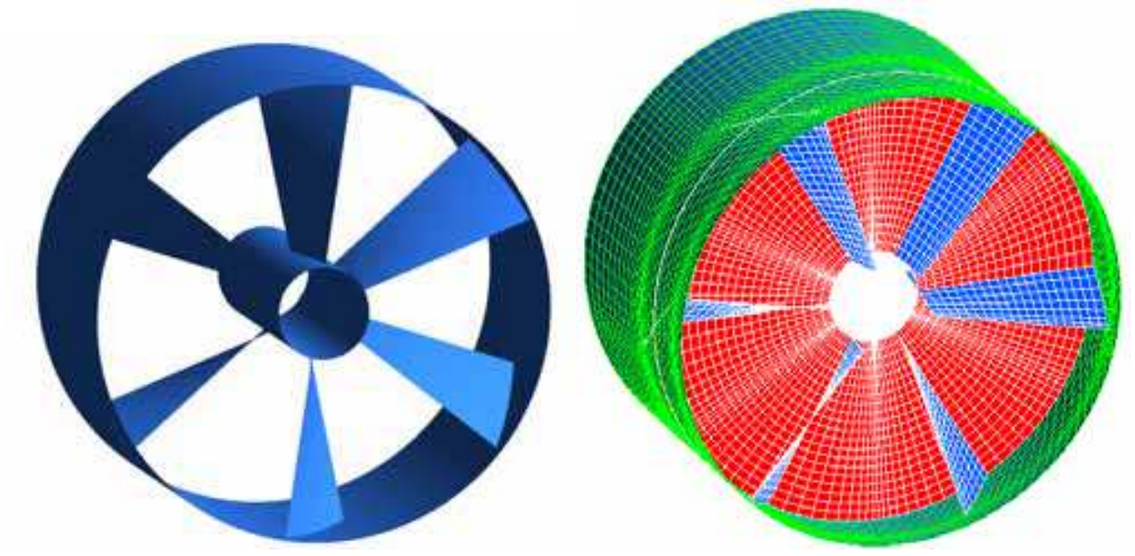


Fig. 24. a) Axial Fan model b) Computational grid

Dozohme (2006) has reported rotating components like fans and blowers contribute to the tonal component, which is very unpleasant. The tonal noise is influenced by the rotational speed of the fan, the number of blades, fan size and mass flow rate through the fan. Tight tolerances between the blades and casing improve overall efficiency. This improved efficiency in turn reduces the overall sound levels; the asymmetrical blade locations reduce the blade passing frequency tones, while generating a smoother sound spectrum. The choice of different hub diameters, hub/tip ratios along with variations in blade span, ensures the economical performance. Focusing on noise analysis, Shao-Yi Hsia (2009) has suggested that there are several paths through which noise may be radiated from the fluid machine require to be controlled.

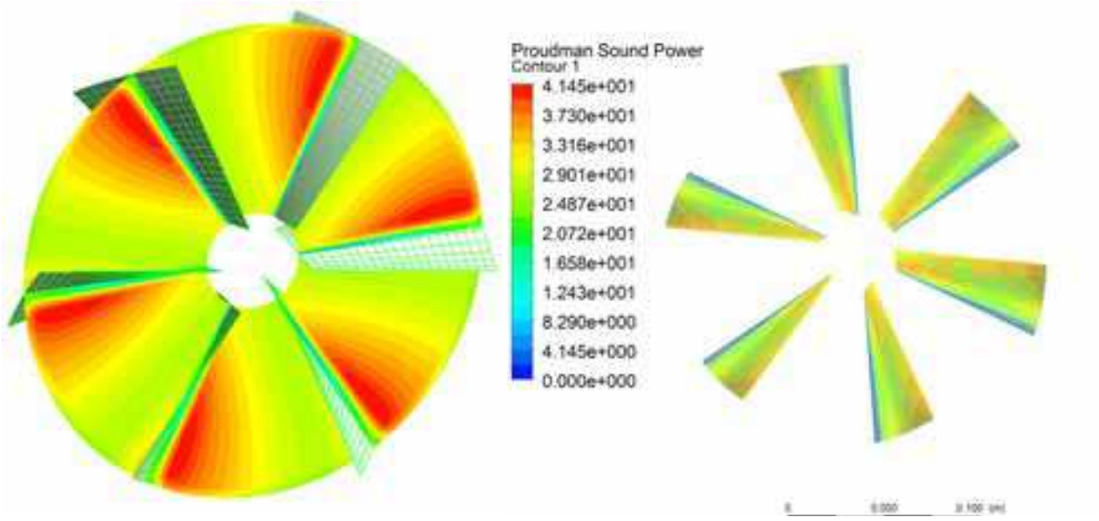


Fig. 25. a) Velocity b) Sound power

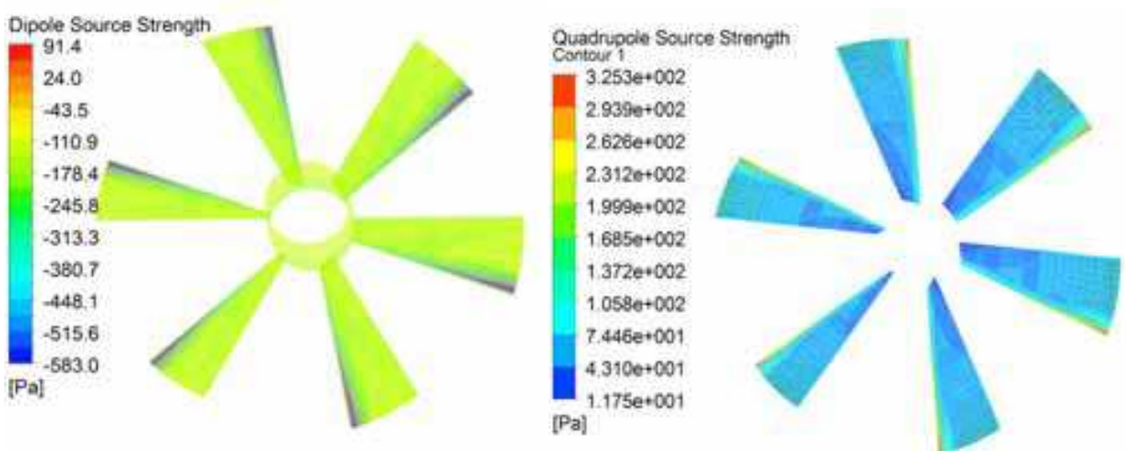


Fig. 26. a) Dipole b) Quadrupole noise source strength

The methodology used is applicable to low Mach number in unsteady flows, where the radiated noise is a small byproduct of the flow that is not altered by it. This assumption is central to Lighthill's formulation of aerodynamic sound generation, which implies that

sound characteristics are obtained in two stages. Turbulent flow fields are predicted at CFD stage followed by sound post-processing stage. One of the objectives of this study is to select turbulence modeling technique that is computationally affordable and yet capable in producing appropriate data for acoustic characteristics.
In order to predict flow and far field noise for the enclosed fan assembly with six blades shown in Fig 24(a) is rotating with 2000 rpm. In order to simulate the flow, a computational grid has been generated for the fan shown in fig 24(b) with boundary condition regions inlet, exit, hub, shroud, blade surfaces, and periodic surfaces in the pre-processor Hypermesh.
The flow simulation has been carried out with defined flow conditions and blade rotations to predict the efficiency of fan. The velocity pattern and sound power on blade surfaces obtained are shown in the Fig-25(a-b). Due to presence of turbulent flow field and blade rotations the dipole and quadruple noise strength variations on the blade surfaces are shown in Fig 26(a-b) using F-W wave equation as a function of flow pressure. From the frequency analysis, it is estimated that overall sound level pressure and sound power are 54.68 dB at 200 Hz respectively are measured at one meter distance from the component. The fan efficiency the ratio between the power transferred to the airflow (outlet – inlet) and the mechanical power consumed by the rotating blades for defined flow conditions are calculated is about 76%. Fan efficiency can be further improved using shape optimization of blades in conjunction with CFD.

10. Optimisation – advance tools in CAD-CFD

Turbo machinery design is a complex task that involves many objectives and constraints coming from different disciplines. Many optimization algorithms have been reported to date with varying degree of success. One of the approaches used for optimization of puffer valve was extensively discussed by C.Srikanth (2009) through unsteady flow simulation with mesh morphing techniques. This technique involves good skills for scripting the moving boundaries in computational model and expensive to perform unsteady state simulations for complex components. In the recent developments more automated methods of shape optimization along with CFD solvers are providing robust tools are discussed by Sheldon Imaoka (2006) through design of experiments using Response Surface Method - RSM. RSM attempts to substitute for the optimizations using iterative flow simulations for variations in geometries by Design of Experiments - DOEs using response surfaces. RSM basically works with linear and non-linear coefficients uses Monte-Carlo simulations for global approximations. Global approximations are very beneficial in case of multi-objective problems; they are built and reformulated based on shapes and constraints. In order to increase marginal efficiency of axial fan, an investigation has been undertaken to simulate the flow inside the fan using mesh morphing, shape optimization and DOE on RSM is under progress based on approach discussed by Nixing Chen (2007. Once the user determines that the generated response surface provide a useful representation of the input-output relationship, goal driven optimization, six sigma analysis or robust design studies then can be performed instead of running time consuming flow simulations for every changed geometry.

11. Concluding remarks

The failures of power plant components used in terms of flow losses, erosive wear by particle impacts, cleaning devices performance due to non-uniform flows and effect of

turbulence in rotating machinery for excessive noise generation are extensively discussed. The alternative approaches are explored to understand the flow behavior involving multiphysics are through CAE for virtual product development. State of art approaches are covered for modeling and grid generation in simple/complex situations with help of programming and commercially available software. Mathematical descriptions for body fitted coordinates, presence of Reynolds's stress due to turbulent flow for development of pressure based algorithms to simulate incompressible fluid flows are briefly outlined. The formulations related to coupled fluid-solid stress and aerodynamic noise is also highlighted to predict structural stresses and far field noise. The case study related to grinding mill has been discussed and also suggested as how the flow recirculation pattern observed in air housing can be minimized by adding two inlet ducts. Complex multiblock grid generation to simulate the turbulent flow through inlet duct with turning vanes of ESP was detailed for flow uniformity using several CFD solvers in second case study. The simulation of fluid-particles present in the cleaning device is outlined in third case study to provide remedies for preventing the flow from one side of the outlet towards convective pass of CFBC power plant used in paper manufacturing unit. A case study of transition duct used in gas turbine is highlighted for flow pattern and its pressure loads on structural stresses/displacements. Pressure fluctuations in turbo machinery components generates excessive noise and the methodology to predict far field noise from an axial fan is described in final case study. RSM with DOE through mesh morphing techniques in conjunction with CFD are suggested as alternatives for optimization to obtain high efficient devices used in power and process equipment.

12. References

Alan Powel, How do vortices generate sound? Acoustic Radiation and Wave Propagation, ASME, NCA vol 17, 1994

Anagnotopoulos J et.al, Numerical Investigation of the grinding process in a beater wheel with classifier, *ASME Journal of Engineering for Gas Turbines and Power*, pages, 1997

Bhasker C et.al, Air Flow Simulation in Electrostatic Precipitator, *BHEL Journal*, Vol 26, No.4, PP:56-61, 2005

Bhasker C, Flow simulation in ESP Duct with turning vanes, revised paper submitted for *Advances in Software Engineering Journal*, Elsevier, UK, 2011.

Bhasker C., CFD applications for Industrial Flow Simualtions – Invited talk, *SONIC-10 Conference*, *International Institute of information Technology*, Pune, India, 2010(a)

Bhasker C., Flow Analysis in Lignite Grinding Mill, *Procgs of 34th National Conference on Fluid Mechanics and Fluid power*, BITS, Ranchi, India, pp 698-702

Bhasker C., Grid Generation for complex industrial components – Lecture notes for a training program on CFD for practicing engineers, IIT, Roorkee, 2010(b).

Bhasker C., Numerical simulation of turbulent flow in complex geometries used in power plants, *Advances in Engineering Software*, vol. 33, pp 71-83, 2001.

Bhasker C., Troubleshooting Steam Turbine By-pass Valves Role of CFD as a Key Analytical Tool Pumps, *Valve and Systems Industrial magazine*, Ahemdabad, India, 2010 (c)

Bhasker, C, Flow simulation in industrial cyclone separator, *Advances in Engineering Software*,Vol 41,issue 2, pp 220-228, 2010

Bhasker, C., Post Doctoral research report on high performance computing, Engineering Research Center, Mississippi State University, Strakville, USA, 2000

Bobcock GH et.al, *Steam and its generation & use*, 41st edition, Chapter-12 Bobcox and Wilcox publishers, USA. 2005

Christopher Riff, Computational Fluid Dynamics Modeling, Laboratory Product/Process Design, University of Chicago, USA, 2004

Davies, D.O et.al. Experimental investigation of turbulent flow through circular to rectangular transition duct, NASA Report TM105210, 1991.

Delli P et.al, Unigraphics for engineering design, Dept. of Mechanical and Aerospace Engineering, Rolla, Missouri, 2007

Dozolme A et. al, Electronics cooling fan noise prediction, *Nice Cote d' Azur seminar*, France, 2006.

Dumont J et.al, Computational Fluid Dynamic Modeling of Electro-static Precipitators, *Procgs of 8th Internation Conference on Electro-static Precipitation*, 2001.

Durbin P.A.: Separated Flow Computations with the k-ε-v^2 Model, *AIAA Journal*, V33, N4, PP659-664, 1995

Efim Korytnyi, et.al, Computational fluid dynamic simulations of coal-fired utility boilers: An engineering tool, *International Journal – Fuel*, paper under press, 2008

Ffowcs W JE, Sound Generation by Turbulence and surfaces in arbitrary motion, *Procgs of Royal Society*, Vol 264, 1969.

Fletcher CAJ, Gas particle industrial flow simulation using RANSTAD, *Sadhana*, Vol 18, Parts 3&4, pp 657-681, 1993

Fraser S M, et. al, Computational and experimental investigations in a cyclone dust separator, *Procgs. of Institution of Mechanical Engineers*, UK, 1997.

Gallimberti, I, Recent advancements in the physical modeling of electrostatic precipitators, *Journal of electrostatics*, vol.43, pp 219-217, 1998

Greschner B et.al, Influence of turbulence modeling on the broadband noise simulation for complex flows, AIAA paper No:902, 2004

H¨auser J et.al, Modern Introduction to Grid Generation, Short course Notes, EPF Lausanne, Dept. of Parallel Computing Center of Logistics/Expert Systems Salzgitter, Deutschland, 1996

Hoffman, K.A et al, Computational Fluid Dynamics for Engineers, in two volumes, *Engineering Education System*, Wichita, KS, 67208-1078. 1993.

Humphery JAC, Fundamentals of fluid motion in erosion by solid particle impact, *Int.Jrnl. Heat & Mass Transfer*, Vol.11, p170, 1990

Iyer VK et. al , Flow Studies through Quick Closing Non-return Valves, *Procs. 2nd Nat. Conf. on CFD applications in Power & industry sector*s, BHEL, Hyderabad, pp 152-155, 2009

Jeff Benoit, Enhancing Gas Turbine Power Plant Profitability Chronic transition piece and turbine part failures. *Power engineering*, Penwel publishers, USA, 2007

Jun Shao, et.al, Turbulence Modeling in Computational Fluid Dynamics (CFD), lecture notes, Maxwell Stanley Hydraulics Laboratory The University of Iowa, 2009

Mandechthild Angleys, Development of modern EVT Bowl Mill, *VGB Power Technology*, Vol 9, pp 60-66, 1998

Maria A et.al, Experimental investigation, of particle motion in a model of a beater wheel mill, *Proceedings, 2nd. Inter. Conf. on Multiphase Flow*, Kyoto, Ja, Vol. 3 PT4, pp. 9-18, 1985

Mustafa A.H, et al, Thermal Stress analysis in annular duct resembling as turbine transition piece, *Journal of Materials processing Technology*, *Elsevier Publishers*,Vol.131,pp283-294, 2006.

Naixing Chen, et.al, Blade Parameterization & Aerodynamic Deisgn optimization, *Procgs. of 8th Int. Symp., exp. Comp., aero-thermo dynamics paper* ISAIF8-8021,Lyon, 2007.

Nlelsen N F et.al, Numerical modelling of gas distribution in electro-static precipitators, *Procgs of 8th International Conference on Electrostatic Precipitators*, 2001.

Pordal H.S et.al. Computational fluid dynamics a key analytical tool, *Hydrocarbon processing*, pp 85-91, 2001

Rajaram S., Design features and operating experience of circulating fluidized bed boilers firing high ash coals in India. *Procs. of the 15th ASME conf. on fluidised bed combustion*; 1999.

Richard H C, Application of the RNS3D Code to a circular –rectangular Transition duct, NASA Report TM 209394, 1999

Routhiainen, P.O et.al, On the Deposition of small particles from Turbulent Streams, *ASME Jr of Heat Transfer*, pp 169-178, 1970

Sandeep Sovani, Accoustic modeling, *CFD Summit 2005*, Fluent Inc., Hampton, USA.

Schmitz W et.al, Computational Fluid Dynamics modeling of Collection Dynamics, *Procgs of 8th International Conference on Electro-Static Preceipitation*, 2001.

Schuh MJ, Numerical predictions of fluid and particle motion in flows past tubes, Ph.D thesis, Univ. of California, USA, 1987.

Shao-Yi Hsia et al , Sound field analysis and simulation for fluid machines, Vol.40, *Advances in Engineering Software*, pp pp 15-22, 2009, Elsevier publishers, UK.

Shekar Majumdar, Pressure based finite volume algorithm for viscous flow computation, Lecture Notes, CFD Advances and Applications, NAL, Bangalore, India, 1994

Sheldon Imaoka, Generating Response Surfaces in Ansys DesignXplorer, *Ansys Solutions*, Vol 7, pp 38-39,2008

Slack .M.D et al, Advances in cyclone modeling using unstructured grids, *Trans IChemE* Vol 78, Part A, 2008

Sodja, J, Turbulence Models in CFD, Internal Report, Departmnet of Physics, University of Ljubljana, 2007.

Spekreijse, S.P et.al, Multiblock grid generation Part I: Elliptic grid generation methods for structured grids, *27th CFD Course*, VonKarman Institute for fluid dynamics, Belgium, 1996

Srikanth C et.al, Flow analysis in valve with moving grids through CFD Techniques Vol.40, *Advances in Engineering Software*, 2009, Elsevier publishers, UK

Srinivas RK , Status of electrostatic precipitator technology usage in India, *Teri inf. Monitor on env. science*, Vol.,pp:1-12, 1996.

St. Petersburg, Introduction to numerical simulation of fluid flows, Lecture notes, University of Munich, Germany, 2004

Stephen Fergusen, Polyhedra: Nature's answer to Meshing, CD-Aadapco, *Dynamics* Vol 25, pp 8-9, 2005.

Suagiyama H, et. al, Numerical Analysis of Turbulent Structure through a circular to Rectangular transition duct, *Procgs of 5th Jnt. Thermal Engineering Conf*, USA, Pap.AJTE99-6385, 1999.

Subramanian SA et.al, Operating Experience of PA, ID & FD Fans affecting the plant load factors of 200/210 MW power plant units, *Seminar on Fans*, Paper No.15, New Delhi, 1984

Tabakoff,W., Performance deterioration of Turbomachinery with presence of solid particles, *Procegs., of AIAA /ASME Joint d heat transfer conference*, St Louis, Missouri, USA, 1982

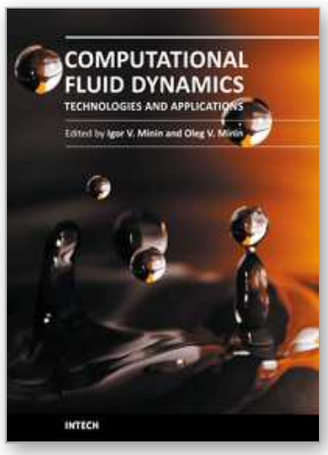
Thompson T B et.al, Chemical Industry of the Future, Technology Road map for Computational Fluid Dynamics, 1996

Thomson, J.F et.al, Numerical Grid Generation – Foundations and Applications, North Holland, Amsterdam, 1985

Varonos A A et.al, Prediction of the cleaning efficiency of an electrostatic precipitator, *Journal of electrostatics*, vol.55, Vol.55, pp 111-133, 2002.

Wilcox, D.C, Turbulence modelling for CFD, *DCW Industries*, California, USA, 1993

Zhiqiang Zhai, et.al, Evaluation of Various Turbulence Models in Predicting Airflow and Turbulence in Enclosed Environments, *HVAC&R Research*, 13(6).2007



Computational Fluid Dynamics Technologies and Applications
Edited by Prof. Igor Minin

ISBN 978-953-307-169-5
Hard cover, 396 pages
Publisher InTech
Published online 05, July, 2011
Published in print edition July, 2011

This book is planned to publish with an objective to provide a state-of-art reference book in the area of computational fluid dynamics for CFD engineers, scientists, applied physicists and post-graduate students. Also the aim of the book is the continuous and timely dissemination of new and innovative CFD research and developments. This reference book is a collection of 14 chapters characterized in 4 parts: modern principles of CFD, CFD in physics, industrial and in castle. This book provides a comprehensive overview of the computational experiment technology, numerical simulation of the hydrodynamics and heat transfer processes in a two dimensional gas, application of lattice Boltzmann method in heat transfer and fluid flow, etc. Several interesting applications area are also discusses in the book like underwater vehicle propeller, the flow behavior in gas-cooled nuclear reactors, simulation odour dispersion around windbreaks and so on.

How to reference
In order to correctly reference this scholarly work, feel free to copy and paste the following:

C. Bhasker (2011). Simulation of Three Dimensional Flows in Industrial Components using CFD Techniques, Computational Fluid Dynamics Technologies and Applications, Prof. Igor Minin (Ed.), ISBN: 978-953-307-169-5, InTech, Available from: http://www.intechopen.com/books/computational-fluid-dynamics-technologies-and-applications/simulation-of-three-dimensional-flows-in-industrial-components-using-cfd-techniques

INTECH
open science | open minds

InTech Europe
University Campus STeP Ri
Slavka Krautzeka 83/A
51000 Rijeka, Croatia
Phone: +385 (51) 770 447
Fax: +385 (51) 686 166
www.intechopen.com

InTech China
Unit 405, Office Block, Hotel Equatorial Shanghai
No.65, Yan An Road (West), Shanghai, 200040, China
中国上海市延安西路65号上海国际贵都大饭店办公楼405单元
Phone: +86-21-62489820
Fax: +86-21-62489821

© 2011 The Author(s). Licensee IntechOpen. This chapter is distributed under the terms of the Creative Commons Attribution-NonCommercial-ShareAlike-3.0 License, which permits use, distribution and reproduction for non-commercial purposes, provided the original is properly cited and derivative works building on this content are distributed under the same license.

IntechOpen

IntechOpen